Maximally symmetric two Higgs doublet model with natural standard model alignment

P.S. Bhupal Dev[a] **and Apostolos Pilaftsis**[a,b]

[a]*Consortium for Fundamental Physics, School of Physics and Astronomy,*
University of Manchester,
Manchester, M13 9PL, United Kingdom

[b]*CERN, Department of Physics, Theory Division,*
CH-1211 Geneva 23, Switzerland

E-mail: bhupal.dev@manchester.ac.uk,
apostolos.pilaftsis@manchester.ac.uk

ABSTRACT: We study the Higgs mass spectrum as predicted by a Maximally Symmetric Two Higgs Doublet Model (MS-2HDM) potential based on the SO(5) group, softly broken by bilinear Higgs mass terms. We show that the lightest Higgs sector resulting from this MS-2HDM becomes naturally aligned with that of the Standard Model (SM), independently of the charged Higgs boson mass and $\tan\beta$. In the context of Type-II 2HDM, SO(5) is the simplest of the *three* possible symmetry realizations of the scalar potential that can naturally lead to the SM alignment. Nevertheless, renormalization group effects due to the hypercharge gauge coupling g' and third-generation Yukawa couplings may break sizeably this alignment in the MS-2HDM, along with the custodial symmetry inherited by the SO(5) group. Using the current Higgs signal strength data from the LHC, which disfavour large deviations from the SM alignment limit, we derive lower mass bounds on the heavy Higgs sector as a function of $\tan\beta$, which can be stronger than the existing limits for a wide range of parameters. In particular, we propose a new collider signal based on the observation of four top quarks to directly probe the heavy Higgs sector of the MS-2HDM during the run-II phase of the LHC.

Contents

1 Introduction

The discovery of a Higgs resonance with mass around 125 GeV at the LHC [1, 2] offers an unprecedented opportunity for probing extended Higgs scenarios beyond the Standard Model (SM). Although the measured properties of the discovered Higgs boson show remarkable consistency with those predicted by the SM [3, 4], the current experimental data still leave open the possibility of new physics that results from an extended Higgs sector. In fact, several well-motivated new-physics scenarios require an enlarged Higgs sector, such as supersymmetry [5], in order to address a number of theoretical and cosmological issues, including the gauge hierarchy problem, the origin of the Dark Matter and the baryon asymmetry in our Universe. Here we follow a modest bottom-up approach and consider one of the simplest Higgs-sector extensions of the SM, namely the Two Higgs Doublet Model (2HDM) [6].

The 2HDM contains two complex scalar fields transforming as iso-doublets $(\mathbf{2}, 1)$ under the SM electroweak gauge group $\mathrm{SU}(2)_L \otimes \mathrm{U}(1)_Y$:

$$\Phi_i = \begin{pmatrix} \phi_i^+ \\ \phi_i^0 \end{pmatrix}, \tag{1.1}$$

with $i = 1, 2$. In this doublet field space $\Phi_{1,2}$, the general 2HDM potential reads

$$
\begin{aligned}
V = & -\mu_1^2(\Phi_1^\dagger \Phi_1) - \mu_2^2(\Phi_2^\dagger \Phi_2) - \left[m_{12}^2(\Phi_1^\dagger \Phi_2) + \text{H.c.} \right] \\
& + \lambda_1(\Phi_1^\dagger \Phi_1)^2 + \lambda_2(\Phi_2^\dagger \Phi_2)^2 + \lambda_3(\Phi_1^\dagger \Phi_1)(\Phi_2^\dagger \Phi_2) + \lambda_4(\Phi_1^\dagger \Phi_2)(\Phi_2^\dagger \Phi_1) \\
& + \left[\frac{1}{2}\lambda_5(\Phi_1^\dagger \Phi_2)^2 + \lambda_6(\Phi_1^\dagger \Phi_1)(\Phi_1^\dagger \Phi_2) + \lambda_7(\Phi_1^\dagger \Phi_2)(\Phi_2^\dagger \Phi_2) + \text{H.c.} \right] , \qquad (1.2)
\end{aligned}
$$

which contains four real mass parameters $\mu_{1,2}^2$, $\text{Re}(m_{12}^2)$, $\text{Im}(m_{12}^2)$, and ten real quartic couplings $\lambda_{1,2,3,4}$, $\text{Re}(\lambda_{5,6,7})$, and $\text{Im}(\lambda_{5,6,7})$. As a consequence, the vacuum structure of the general 2HDM can be quite rich [7], and in principle, can allow for a wide range of parameter space still compatible with the existing LHC constraints. However, additional requirements, such as the Glashow–Weinberg condition [8, 9], must be imposed, so as to avoid Higgs interactions with unacceptably large flavour changing neutral currents (FCNC) at the tree level. The Glashow–Weinberg condition is satisfied by four discrete choices of tree-level Yukawa couplings between the Higgs doublets and SM fermions.[1] By performing global fits to the current Higgs signals at the LHC and Tevatron in terms of the 2HDM parameter space, it has been shown [11–18] that all four discrete 2HDM types are constrained to lie close to the so-called SM *alignment limit*, in which the mass eigenbasis of the CP-even scalar sector aligns with the SM gauge eigenbasis. Specifically, in the Type-II (MSSM-type) 2HDM, the coupling of the SM-like Higgs to vector bosons is constrained to lie within 10% of the SM value at 95% CL [14, 19–22].

In light of the present and upcoming LHC data, possible mechanisms that lead to the SM alignment limit within the 2HDM require further investigation and scrutiny. Naively, the SM alignment limit is often associated with the decoupling limit, in which all the non-standard Higgs bosons are assumed to be much heavier than the electroweak scale so that the lightest CP-even scalar behaves like the SM Higgs boson. This SM alignment limit can also be achieved, without decoupling [23–26].[2] However, for small $\tan\beta$ values, this is usually attributed to accidental cancellations in the 2HDM potential [26].

In this paper, we seek a symmetry of the 2HDM potential to naturally justify the alignment limit, without decoupling, independently of the kinematic parameters of the theory, such as the charged Higgs mass and $\tan\beta$. We show that a Maximally Symmetric 2HDM (MS-2HDM) potential based on the SO(5) group can *naturally* realize the alignment limit, where SO(5) acts on a bilinear field space to be discussed in section 2. In section 3, we show that, in the context of Type-II 2HDM, the maximal symmetry group SO(5) is the simplest of the *three* possible symmetry realizations of the scalar potential having natural alignment. Nevertheless, as we analyze in section 3, renormalization group (RG) effects due to the hypercharge gauge coupling g' and third-generation Yukawa couplings, as well as soft-breaking mass parameters, violate explicitly the SO(5) symmetry, thereby inducing relevant deviations from the alignment limit. As we discuss in section 4, such deviations

---

[1]In general, the absence of tree-level flavour-changing couplings of the neutral scalar fields can be guaranteed by requiring the Yukawa coupling matrices to be aligned in flavour space [10].

[2]A similar situation was also discussed in an extension of the MSSM with a triplet scalar field [27], where alignment without decoupling could be achieved in a parameter region at small $\tan\beta \lesssim 10$.

lead to distinct predictions for the Higgs spectrum of the MS-2HDM. In section 5, we present a novel collider signature of the MS-2HDM with four top quarks as final states. In section 6 we present our conclusions. Finally, several technical details related to our study have been relegated to appendices A and B.

2 Maximally symmetric two Higgs doublet model potential

In order to identify all accidental symmetries of the 2HDM potential, it is convenient to introduce the 8-dimensional complex multiplet [7, 28, 29]:

$$
\mathbf{\Phi} \equiv \begin{pmatrix} \Phi_1 \\ \Phi_2 \\ \widetilde{\Phi}_1 \\ \widetilde{\Phi}_2 \end{pmatrix} ,
\tag{2.1}
$$

where $\widetilde{\Phi}_i = \mathrm{i}\sigma^2\Phi_i^*$ (with $i = 1, 2$) and σ^2 is the second Pauli matrix. We should remark that the complex multiplet $\mathbf{\Phi}$ satisfies the Majorana property [7]: $\mathbf{\Phi} = C\mathbf{\Phi}^*$, where $C = \sigma^2 \otimes \sigma^0 \otimes \sigma^2$ is the charge-conjugation matrix, with $\sigma^0 = \mathbf{1}_{2\times2}$ being the identity matrix. In terms of the $\mathbf{\Phi}$-multiplet, the following *null* 6-dimensional Lorentz vector can be defined [7, 29]:

$$
R^A \equiv \mathbf{\Phi}^\dagger \Sigma^A \mathbf{\Phi} ,
\tag{2.2}
$$

where $A = 0, 1, \ldots, 5$ and the six 8×8-dimensional matrices Σ^A may be expressed in terms of the three Pauli matrices $\sigma^{1,2,3}$, as follows:

$$
\begin{aligned}
\Sigma^{0,1,3} &= \frac{1}{2}\sigma^0 \otimes \sigma^{0,1,3} \otimes \sigma^0, \quad \Sigma^2 = \frac{1}{2}\sigma^3 \otimes \sigma^2 \otimes \sigma^0, \\
\Sigma^4 &= -\frac{1}{2}\sigma^2 \otimes \sigma^2 \otimes \sigma^0, \quad \Sigma^5 = -\frac{1}{2}\sigma^1 \otimes \sigma^2 \otimes \sigma^0.
\end{aligned}
\tag{2.3}
$$

We must emphasize here that the bilinear field space spanned by the 6-vector R^A realizes an *orthochronous* $\mathrm{SO}(1,5)$ symmetry group.

In terms of the 6-vector R^A defined in (2.2), the 2HDM potential V given in (1.2) takes on a simple quadratic form:

$$
V = -\frac{1}{2}M_A R^A + \frac{1}{4}L_{AB}R^A R^B ,
\tag{2.4}
$$

where M_A and L_{AB} are $\mathrm{SO}(1,5)$ constant 'tensors' that depend on the mass parameters and quartic couplings of the scalar potential V and their explicit forms may be found in [29–32]. Requiring that the $\mathrm{SU}(2)_L$ gauge-kinetic term of the multiplet $\mathbf{\Phi}$ remains canonical restricts the allowed set of rotations from SO(1,5) to SO(5),[3] where only the spatial components R^I (with $I = 1, \ldots, 5$) transform, whereas the zeroth component R^0 remains invariant. Consequently, in the absence of the hypercharge gauge coupling g' and fermion Yukawa

---

[3]We note in passing that if the restriction of $\mathrm{SU}(2)_L$ gauge invariance is lifted, the 2HDM is then equivalent to an *ungauged* theory with 8 real scalars and so the maximal symmetry group becomes the larger group O(8) [33].

couplings, the maximal symmetry group of the 2HDM is $G^R_{2\text{HDM}} = \text{SO}(5)$. Given the group isomorphy $\text{SO}(5) \sim \text{Sp}(4)/\text{Z}_2$, the maximal symmetry group of the 2HDM in the original $\mathbf{\Phi}$-field space is [29][4]

$$G^{\mathbf{\Phi}}_{2\text{HDM}} = (\text{Sp}(4)/\text{Z}_2) \otimes \text{SU}(2)_L \,, \qquad (2.5)$$

in the custodial symmetry limit of vanishing g' and fermion Yukawa couplings. The quotient factor Z_2 in (2.5) is needed to avoid double covering the group $G^{\mathbf{\Phi}}_{2\text{HDM}}$ in the $\mathbf{\Phi}$-space. One may note here that the 10 Lie generators of $\text{Sp}(4)$ may be represented in the $\mathbf{\Phi}$-space as $K^a = \kappa^a \otimes \sigma^0$ (with $a = 0, 1, 2, \ldots, 9$), where

$$
\begin{aligned}
\kappa^0 &= \frac{1}{2}\,\sigma^3 \otimes \sigma^0 \,, & \kappa^1 &= \frac{1}{2}\,\sigma^3 \otimes \sigma^1 \,, \\
\kappa^2 &= \frac{1}{2}\,\sigma^0 \otimes \sigma^2 \,, & \kappa^3 &= \frac{1}{2}\,\sigma^3 \otimes \sigma^3 \,, \\
\kappa^4 &= \frac{1}{2}\,\sigma^1 \otimes \sigma^0 \,, & \kappa^5 &= \frac{1}{2}\,\sigma^1 \otimes \sigma^3 \,, \\
\kappa^6 &= \frac{1}{2}\,\sigma^2 \otimes \sigma^0 \,, & \kappa^7 &= \frac{1}{2}\,\sigma^2 \otimes \sigma^3 \,, \\
\kappa^8 &= \frac{1}{2}\,\sigma^1 \otimes \sigma^1 \,, & \kappa^9 &= \frac{1}{2}\,\sigma^2 \otimes \sigma^1 \,,
\end{aligned}
\qquad (2.6)
$$

with the normalization: $\text{Tr}(\kappa^a \kappa^b) = \delta^{ab}$. Thus, the group $G^{\mathbf{\Phi}}_{2\text{HDM}}$ includes the $\text{U}(1)_Y$ hypercharge group through the $\text{Sp}(4)$ generator K^0, whereas the 9 other $\text{Sp}(4)$ generators listed in (2.6) are related to various Higgs Family and CP transformations [29]. On the other hand, the $\text{SU}(2)_L$ generators in the $\mathbf{\Phi}$-space may be written as $\sigma^0 \otimes \sigma^0 \otimes (\sigma^b/2)$ (with $b = 1, 2, 3$), which manifestly commute with all $\text{Sp}(4)$ generators K^a.

As we will see below by an explicit construction [cf. (2.9) and section 2.1], it is not difficult to deduce that, in the custodial symmetry limit, the maximal symmetry group for an n Higgs Doublet Model (nHDM) will be

$$G^{\mathbf{\Phi}}_{n\text{HDM}} = (\text{Sp}(2n)/\text{Z}_2) \otimes \text{SU}(2)_L \,, \qquad (2.7)$$

in which case the multiplet $\mathbf{\Phi}$ becomes a Majorana $4n$-dimensional complex vector.[5] It is interesting to note that for the SM with $n = 1$ Higgs doublet, (2.7) yields the well-known result: $G^{\mathbf{\Phi}}_{\text{SM}} = (\text{SU}(2)_C/\text{Z}_2) \otimes \text{SU}(2)_L$, by virtue of the group isomorphy: $\text{Sp}(2) \sim \text{SU}(2)_C$, where $\text{SU}(2)_C$ is the custodial symmetry group originally introduced in [36]. Hence, it is important to stress that (2.7) represents a general result that holds for any nHDM.

We may now identify all maximal symmetries of the 2HDM potential by classifying all proper, improper and semi-simple subgroups of $\text{SO}(5)$ in the bilinear R^I space. In this way, it was found [7, 29] that a 2HDM potential invariant under $\text{SU}(2)_L \otimes \text{U}(1)_Y$ can possess a maximum of 13 accidental symmetries. This symmetry classification extends the

---

[4]In [29], the symplectic group $\text{Sp}(4)$ is denoted as $\text{SU}_M(4)$, where the 10 generators of the restricted $\text{U}(4)$ group satisfying a Majorana (symplectic) condition were presented.

[5]Given an apparently deep connection between $\text{SO}(2n + 1)$ and $\text{Sp}(2n)$ groups [34, 35], both of which have $n(2n+1)$ generators, one might be able to identify the necessary bilinears in the R-space for an nHDM. However, this is somewhat non-trivial for $n \geq 3$, and therefore, we postpone this discussion to a future dedicated study.

previous list of six symmetries reported in [31], where possible custodial symmetries of the theory were not included. Each of the 13 classified symmetries puts some restrictions on the kinematic parameters appearing in the 2HDM potential (1.2). In a specific diagonally reduced bilinear basis [37, 38], one has the general restrictions $\text{Im}(\lambda_5) = 0$ and $\lambda_6 = \lambda_7$, thus reducing the number of independent quartic couplings to seven. In the maximally symmetric SO(5) ($\sim$ Sp(4)/Z_2) limit, we have the following relations between the scalar potential parameters [7, 29]:

$$\mu_1^2 = \mu_2^2, \quad m_{12}^2 = 0,$$
$$\lambda_2 = \lambda_1, \quad \lambda_3 = 2\lambda_1, \quad \lambda_4 = \text{Re}(\lambda_5) = \lambda_6 = \lambda_7 = 0. \tag{2.8}$$

Thus, in the SO(5) limit, the 2HDM potential (1.2) is parametrized by a *single* mass parameter μ^2 and a *single* quartic coupling λ:

$$V = -\mu^2 \left(|\Phi_1|^2 + |\Phi_2|^2\right) + \lambda \left(|\Phi_1|^2 + |\Phi_2|^2\right)^2$$
$$= -\frac{\mu^2}{2} \boldsymbol{\Phi}^\dagger \boldsymbol{\Phi} + \frac{\lambda}{4} \left(\boldsymbol{\Phi}^\dagger \boldsymbol{\Phi}\right)^2. \tag{2.9}$$

It is worth stressing that the MS-2HDM scalar potential in (2.9) is more minimal than the respective potential of the MSSM at the tree level. Even in the custodial symmetric limit $g' \to 0$, the latter only possesses a smaller symmetry: O(2) $\otimes$ O(3) $\subset$ SO(5), in the 5-dimensional bilinear R^I space.

2.1 Custodial symmetries in the MS-2HDM

It is now interesting to discuss the implications of custodial symmetries for the Yukawa sector of the 2HDM. To this end, let us only consider the quark Yukawa sector of the theory, even though it is straightforward to extend our results to the lepton sector as well. The relevant part of the quark-Yukawa Lagrangian in the 2HDM can generally be written down as follows:

$$-\mathcal{L}_Y^q = \bar{Q}_L(h_1^u \Phi_1 + h_2^u \Phi_2)u_R + \bar{Q}_L(h_1^d \widetilde{\Phi}_1 + h_2^d \widetilde{\Phi}_2)d_R$$
$$= (\bar{u}_L, \bar{d}_L) \left(\Phi_1, \Phi_2, \widetilde{\Phi}_1, \widetilde{\Phi}_2\right) \mathcal{H} \begin{pmatrix} u_R \\ d_R \end{pmatrix}, \tag{2.10}$$

where $Q_L \equiv (u_L, d_L)^\mathsf{T}$ is the SM quark iso-doublet and we have introduced a 12×6-dimensional *non*-square Yukawa coupling matrix

$$\mathcal{H} \equiv \begin{pmatrix} h_1^u & \mathbf{0}_{3\times 3} \\ h_2^u & \mathbf{0}_{3\times 3} \\ \mathbf{0}_{3\times 3} & h_1^d \\ \mathbf{0}_{3\times 3} & h_2^d \end{pmatrix}. \tag{2.11}$$

All the custodial symmetries of the 2HDM potential can be deduced by examining the Sp(4) generators $K^a = \kappa^a \otimes \sigma^0$ in the $\boldsymbol{\Phi}$-space, where κ^a are explicitly given in (2.6). Candidate Sp(4) generators of the custodial symmetry are those generators that do *not*

commute with the hypercharge generator K^0, i.e. K^a with $a = 4, 5, 6, 7, 8, 9$. It is not difficult to see that these six generators, together with K^0, form *three* inequivalent realizations of the SU(2)$_C$ custodial symmetry [29]: (i) $K^{0,4,6}$, (ii) $K^{0,5,7}$ and (iii) $K^{0,8,9}$.

In order to see the implications of the three custodial symmetries (i), (ii) and (iii) for the quark Yukawa sector, we impose a symmetry commutation relation on $\mathcal{H}$ after generalizing it for *non*-square matrices:

$$\kappa^a \mathcal{H} \; - \; \mathcal{H} t^b \; = \; \mathbf{0}_{4 \times 2} \, , \qquad (2.12)$$

where $\mathcal{H}$ is expressed in the reduced 4×2-dimensional space, in which the 3×3 flavour space has been suppressed. In addition, we denote with $t^b = \sigma^b/2$ (with $b = 1, 2, 3$) the three 2×2 generators of the custodial SU(2)$_C$ group. One can immediately check that it holds $\kappa^0 \mathcal{H} - \mathcal{H} t^3 = \mathbf{0}_{4 \times 2}$, which implies that the specific block structure of $\mathcal{H}$ in (2.11) respects U(1)$_Y$ by construction, given the correspondence: $\kappa^0 \leftrightarrow t^3$. In detail, imposing (2.12) for the three SU(2)$_C$ symmetries, we obtain the following relations among the 3×3 up- and down-type quark Yukawa coupling matrices:

$$
\begin{aligned}
\text{(i)} \quad & h_1^u \; = \; e^{i\theta} h_1^d \quad \text{and} \quad h_2^u \; = \; e^{i\theta} h_2^d \, , \\
\text{(ii)} \quad & h_1^u \; = \; e^{i\theta} h_1^d \quad \text{and} \quad h_2^u \; = \; -e^{i\theta} h_2^d \, , \\
\text{(iii)} \quad & h_1^u \; = \; e^{i\theta} h_2^d \quad \text{and} \quad h_2^u \; = \; e^{-i\theta} h_1^d \, ,
\end{aligned}
\qquad (2.13)
$$

where θ is an arbitrary angle unspecified by the symmetry constraint (2.12). We should stress again that only for a fully SO(5)-symmetric 2HDM, the three sets of solutions in (2.13) are equivalent. However, this is not in general true for scenarios that happen to realize only subgroups of SO(5), according to the symmetry classification given in [7, 29].

2.2 Scalar spectrum in the MS-2HDM

The masses and mixing in the Higgs sector of a general 2HDM are given in appendix A. After electroweak symmetry breaking in the MS-2HDM, we have the breaking pattern

$$\text{SO}(5) \; \xrightarrow{\langle \Phi_{1,2} \rangle \neq 0} \; \text{SO}(4) \, , \qquad (2.14)$$

which gives rise to a Higgs boson H with mass $M_H^2 = 2\lambda_2 v^2$, whilst the remaining four scalar fields, denoted hereafter as h, a and $h^\pm$, are massless (pseudo)-Goldstone bosons. The latter is a consequence of the Goldstone theorem [39] and can be readily verified by means of (2.8) in (A.5). Thus, we identify H as the SM-like Higgs boson with the mixing angle $\alpha = \beta$ [cf. (A.7)]. We call this the SM *alignment limit*, which can be naturally attributed to the SO(5) symmetry of the theory.

In the exact SO(5)-symmetric limit, the scalar spectrum of the MS-2HDM is experimentally unacceptable, as the four massless pseudo-Goldstone particles, viz. h, a and $h^\pm$, have sizeable couplings to the SM Z and $W^\pm$ bosons [cf. (A.9)]. These couplings induce additional decay channels, such as $Z \to ha$ and $W^\pm \to h^\pm h$, which are experimentally excluded [40]. Nevertheless, as we will see in the next section, the SO(5) symmetry of the original theory may be violated predominantly by RG effects due to g' and third-generation Yukawa couplings, as well as by soft SO(5)-breaking mass parameters, thereby lifting the masses of these pseudo-Goldstone particles.

3 RG and soft breaking effects

As discussed in the previous section, the SO(5) symmetry that governs the MS-2HDM will be broken due to g' and Yukawa coupling effects, similar to the breaking of custodial symmetry in the SM. Therefore, an interesting question will be to explore whether these effects are sufficient to yield a viable Higgs spectrum at the weak scale. To address this question in a technically natural manner, we assume that the SO(5) symmetry is realized at some high scale μ_X. The physical mass spectrum at the electroweak scale is then obtained by the RG evolution of the 2HDM parameters given by (1.2). Using state-of-the-art two-loop RG equations given in appendix B, we examine the deviation of the Higgs spectrum from the SO(5)-symmetric limit due to g' and Yukawa coupling effects. This is illustrated in figure 1 for a typical choice of parameters in a Type-II realization of the 2HDM, even though the conclusions drawn from this figure have more general applicability. In particular, we obtain the following breaking pattern starting from a $\mathrm{SU(2)}_L$-gauged theory:

$$
\begin{aligned}
\mathrm{SO(5)} \otimes \mathrm{SU(2)}_L \quad &\xrightarrow{g' \neq 0} \quad \mathrm{O(3)} \otimes \mathrm{O(2)} \otimes \mathrm{SU(2)}_L \ \sim \ \mathrm{O(3)} \otimes \mathrm{U(1)}_Y \otimes \mathrm{SU(2)}_L \\
&\xrightarrow{\text{Yukawa}} \quad \mathrm{O(2)} \otimes \mathrm{U(1)}_Y \otimes \mathrm{SU(2)}_L \ \sim \ \mathrm{U(1)}_{\mathrm{PQ}} \otimes \mathrm{U(1)}_Y \otimes \mathrm{SU(2)}_L \\
&\xrightarrow{\langle \Phi_{1,2} \rangle \neq 0} \quad \mathrm{U(1)}_{\mathrm{em}} \,,
\end{aligned}
\tag{3.1}
$$

where $\mathrm{U(1)}_{\mathrm{em}}$ is the electromagnetic group. In other words, RG-induced g' effects only lift the charged Higgs-boson mass $M_{h^\pm}$, while the corresponding Yukawa coupling effects also lift slightly the mass of the non-SM CP-even pseudo-Goldstone boson h. However, they still leave the CP-odd scalar a massless (see left panel of figure 1 for $m_{12}^2 = 0$), which can be identified as a $\mathrm{U(1)}_{\mathrm{PQ}}$ axion [41]. The deviation of the scalar quartic couplings from the SO(5)-symmetric limit given in (2.8), thanks to g' and Yukawa coupling effects, is illustrated in figure 1 (right panel) for a simple choice of the single quartic coupling $\lambda = 0$ at the SO(5)-symmetry scale μ_X.

Figure 1 (left panel) also shows that g' and Yukawa coupling effects are *not* sufficient to yield a viable Higgs spectrum at the weak scale, starting from a SO(5)-invariant boundary condition at some high scale μ_X. To minimally circumvent this problem, we need to include soft SO(5)-breaking effects, by assuming a non-zero value for $\mathrm{Re}(m_{12}^2)$ in the 2HDM potential (1.2). In the SO(5)-symmetric limit (2.8) for the scalar quartic couplings, but with $\mathrm{Re}(m_{12}^2) \neq 0$, we obtain the following mass spectrum [cf. (A.5)]:

$$
M_H^2 \ = \ 2\lambda_2 v^2 \,, \qquad M_h^2 \ = \ M_a^2 \ = \ M_{h^\pm}^2 \ = \ \frac{\mathrm{Re}(m_{12}^2)}{s_\beta c_\beta} \,,
\tag{3.2}
$$

as well as an equality between the CP-even and CP-odd mixing angles: $\alpha = \beta$, thus predicting an *exact* alignment for the SM-like Higgs boson H, simultaneously with an experimentally allowed heavy Higgs spectra (see left panel of figure 1 for $m_{12}^2 \neq 0$). Note that in the alignment limit, the heavy Higgs sector is exactly degenerate [cf. (3.2)] at the SO(5) symmetry-breaking scale, and at the low-energy scale, this degeneracy is mildly broken by the RG effects. Thus, we obtain a quasi-degenerate heavy Higgs spectrum in the MS-2HDM, as illustrated in figure 1 (left panel). We emphasize that this is a
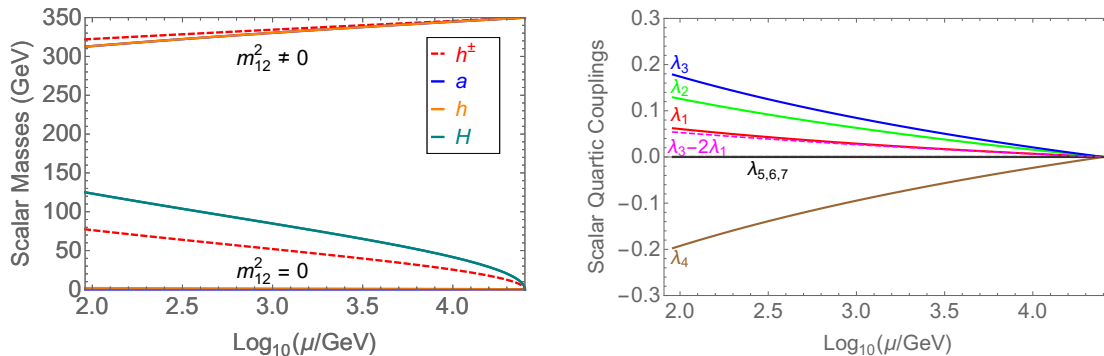
Figure 1. (left panel) The Higgs spectrum in the MS-2HDM without and with soft breaking effects induced by m_{12}^2. For $m_{12}^2 = 0$, the pseudo-Goldstone boson a remains massless at tree-level, whereas h and $h^\pm$ receive small masses due to the g' and Yukawa coupling effects. For $m_{12}^2 \neq 0$, one obtains a quasi-degenerate heavy Higgs spectrum, cf. (3.2). (right panel) The RG evolution of the scalar quartic couplings under g' and Yukawa coupling effects. Here we have chosen $\mu_X = 2.5 \times 10^4$ GeV, $\lambda(\mu_X) = 0$ and $\tan\beta = 50$ for illustration.

unique prediction of this model, valid even in the non-decoupling limit, and can be used to distinguish it from other 2HDM scenarios.

From (3.2), we notice that the alignment limit $\alpha = \beta$ is independent of the charged Higgs-boson mass $M_{h^\pm}$ and the value of $\tan\beta$. This is achieved without *decoupling*, i.e. without the need to consider the mass hierarchy $M_{h^\pm} \gg v$. Hence, in this softly broken SO(5) 2HDM, we get *natural* SM alignment, *without* decoupling.[6] It is instructive to analyze this last point in more detail. In the general CP-conserving 2HDM, the CP-even scalar mass matrix can be written down as [42, 43]

$$
\begin{aligned}
M_S^2 &= M_a^2 \begin{pmatrix} s_\beta^2 & -s_\beta c_\beta \\ -s_\beta c_\beta & c_\beta^2 \end{pmatrix} + v^2 \begin{pmatrix} 2\lambda_1 c_\beta^2 + \lambda_5 s_\beta^2 + 2\lambda_6 s_\beta c_\beta & \lambda_{34} s_\beta c_\beta + \lambda_6 c_\beta^2 + \lambda_7 s_\beta^2 \\ \lambda_{34} s_\beta c_\beta + \lambda_6 c_\beta^2 + \lambda_7 s_\beta^2 & 2\lambda_2 s_\beta^2 + \lambda_5 c_\beta^2 + 2\lambda_7 s_\beta c_\beta \end{pmatrix} \\
&\equiv \begin{pmatrix} c_\beta & -s_\beta \\ s_\beta & c_\beta \end{pmatrix} \widehat{M_S^2} \begin{pmatrix} c_\beta & s_\beta \\ -s_\beta & c_\beta \end{pmatrix},
\end{aligned}
\tag{3.3}
$$

where M_a^2 is given in (A.5), $\lambda_{34} \equiv \lambda_3 + \lambda_4$, and

$$
\widehat{M_S^2} = \begin{pmatrix} \widehat{A} & \widehat{C} \\ \widehat{C} & \widehat{B} \end{pmatrix},
\tag{3.4}
$$

with

$$
\widehat{A} = 2v^2 \left[c_\beta^4 \lambda_1 + s_\beta^2 c_\beta^2 \lambda_{345} + s_\beta^4 \lambda_2 + 2s_\beta c_\beta \left(c_\beta^2 \lambda_6 + s_\beta^2 \lambda_7 \right) \right],
\tag{3.5}
$$

$$
\widehat{B} = M_a^2 + \lambda_5 v^2 + 2v^2 \left[s_\beta^2 c_\beta^2 \left(\lambda_1 + \lambda_2 - \lambda_{345} \right) - s_\beta c_\beta \left(c_\beta^2 - s_\beta^2 \right) \left(\lambda_6 - \lambda_7 \right) \right],
\tag{3.6}
$$

$$
\widehat{C} = v^2 \left[s_\beta^3 c_\beta \left(2\lambda_2 - \lambda_{345} \right) - c_\beta^3 s_\beta \left(2\lambda_1 - \lambda_{345} \right) + c_\beta^2 \left(1 - 4s_\beta^2 \right) \lambda_6 + s_\beta^2 \left(4c_\beta^2 - 1 \right) \lambda_7 \right].
\tag{3.7}
$$

---

[6]Strictly speaking, there will be one-loop threshold corrections to the effective MS-2HDM potential, sourced from a non-zero $\text{Re}(m_{12}^2)$, which might lead to small misalignments. A simple estimate suggests that these corrections are of order $\lambda^2/(16\pi^2)$ and can therefore be safely neglected to a good approximation.

Here we have used the short-hand notation: $\lambda_{345} \equiv \lambda_3 + \lambda_4 + \lambda_5$. Observe that $\widehat{M}_S^2$ in (3.3) is the respective 2×2 CP-even mass matrix written down in the so-called Higgs eigenbasis [44–47].

Evidently, the SM alignment limit $\alpha \to \beta$ for the CP-even scalar mixing angle α is obtained, provided the off-diagonal elements of $\widehat{M}_S^2$ in (3.4) vanish, i.e. for $\widehat{C} = 0$ [24]. From (3.7), this yields the quartic equation

$$\lambda_7 t_\beta^4 - (2\lambda_2 - \lambda_{345})t_\beta^3 + 3(\lambda_6 - \lambda_7)t_\beta^2 + (2\lambda_1 - \lambda_{345})t_\beta - \lambda_6 \;=\; 0 \;. \qquad (3.8)$$

In order to satisfy (3.8) for *any* value of $\tan\beta$, the coefficients of the polynomial in $\tan\beta$ must identically vanish.[7] Imposing this restriction, we conclude that all natural alignment solutions must satisfy the following condition:

$$\lambda_1 \;=\; \lambda_2 \;=\; \lambda_{345}/2 \;, \qquad \lambda_6 \;=\; \lambda_7 \;=\; 0 \;. \qquad (3.9)$$

In particular, for $\lambda_6 = \lambda_7 = 0$, (3.8) has a solution

$$\tan^2\beta \;=\; \frac{2\lambda_1 - \lambda_{345}}{2\lambda_2 - \lambda_{345}} \;>\; 0 \;, \qquad (3.10)$$

independent of M_a. After some algebra, the simple solution (3.10) to our general alignment condition (3.8) can be shown to be equivalent to that derived in [26, 48].

In the alignment limit, the two CP-even Higgs masses are given by the diagonal elements of $\widehat{M}_S^2$ in (3.4):

$$M_H^2 \;=\; 2v^2(\lambda_1 c_\beta^4 + \lambda_{345} s_\beta^2 c_\beta^2 + \lambda_2 s_\beta^4) \;\equiv\; \lambda_{\rm SM} v^2 \;, \qquad (3.11)$$

$$M_h^2 \;=\; M_a^2 \;+\; \lambda_5 v^2 \;+\; 2v^2 s_\beta^2 c_\beta^2 (\lambda_1 + \lambda_2 - \lambda_{345}) \;. \qquad (3.12)$$

On the other hand, in the limit $M_a \gg v$, we can use a seesaw-like approximation in (3.4) to obtain

$$M_H^2 \;\simeq\; \lambda_{\rm SM} v^2 - \frac{v^4 s_\beta^2 c_\beta^2}{M_a^2 + \lambda_5 v^2} \left[s_\beta^2 \Big(2\lambda_2 - \lambda_{345} \Big) - c_\beta^2 \Big(2\lambda_1 - \lambda_{345} \Big) \right]^2 \;, \qquad (3.13)$$

$$M_h^2 \;\simeq\; M_a^2 + \lambda_5 v^2 \;\gg\; v^2 \;. \qquad (3.14)$$

In (3.13) and (3.14), we have also included the possibility of decoupling via a large λ_5 coupling [25]. For large values of $\tan\beta$, e.g. $\tan\beta \gtrsim 10$, we readily see that (3.13) reduces to $M_H^2 \simeq 2\lambda_2 v^2$, which again leads to a natural alignment.

As noted above, in the SO(5) symmetric limit of the conformal part of the 2HDM as given by (2.8) and (3.2), the SM alignment is achieved for any value of $\tan\beta$ [cf. (3.10)]. In addition to SO(5), one may now wonder whether there are other classified symmetries of the 2HDM that lead to natural SM alignment, *independently* of $\tan\beta$ and M_a. According to the classification given in table 1 of [29], we observe that, in the context of Type-II

---

[7]Notice that (3.8) is satisfied automatically in the SO(5) limit given in (2.8).

2HDM, there are *only* two other symmetries which lead to such natural SM alignment by satisfying (3.9), viz.[8]

$$\text{(i)} \quad \text{O}(3) \otimes \text{O}(2): \quad \lambda_1 = \lambda_2 = \lambda_{34}/2, \quad \lambda_5 = \lambda_6 = \lambda_7 = 0, \quad (3.15)$$

$$\text{(ii)} \quad \text{Z}_2 \otimes [\text{O}(2)]^2: \quad \lambda_1 = \lambda_2 = \lambda_{345}/2, \quad \lambda_6 = \lambda_7 = 0. \quad (3.16)$$

Both these symmetries also require $\mu_1^2 = \mu_2^2$ and $m_{12}^2 = 0$. Note that in all the three naturally aligned scenarios, cf. (2.8), (3.15) and (3.16), $\tan\beta$ as given in (3.10) 'consistently' gives an *indefinite* answer 0/0. After spontaneous electroweak symmetry breaking, symmetry (i) predicts two pseudo-Goldstone bosons (h, a), whilst symmetry (ii) predicts only one pseudo-Goldstone boson, i.e. the CP-even Higgs boson h. However, a non-zero soft SO(5)-breaking mass parameter m_{12}^2 can be introduced to render the pseudo-Goldstone bosons sufficiently massive, in agreement with present experimental data, similar to the SO(5) case shown in figure 1. Even though the 2HDM scenarios based on the symmetries (i) and (ii) may be analyzed in a similar fashion, our focus here will be on the simplest realization of the SM alignment, namely, the MS-2HDM based on the SO(5) group. Nevertheless, the results that we will be deriving in the present study are quite generic and could apply to the less symmetric cases (i) and (ii) above as well.

Before concluding this section, we would like to comment that no CP violation is possible in the MS-2HDM, be it spontaneously or explicitly, at least up to one-loop level. This is due to the fact that the Higgs potential (2.9) remains CP-invariant after the RG and one-loop threshold effects, even if a generic soft Z_2-breaking term $\text{Im}(m_{12}^2 e^{i\xi}) \neq 0$ with an arbitrary CP-phase ξ is present. In particular, as illustrated in figure 1 (right panel), a non-zero $\lambda_{5,6,7}$ cannot be induced via RG effects, and this is true to any order in perturbation theory. On the other hand, one-loop threshold effects could induce non-zero $\lambda_{5,6,7}$ of the following form:

$$\lambda_5 \sim \frac{\lambda_3^2 (m_{12}^2)^2}{16\pi^2 |m_{12}^2|^2}, \qquad \lambda_6 \sim \frac{\lambda_1 \lambda_3 m_{12}^2}{16\pi^2 |m_{12}^2|}, \qquad \lambda_7 \sim \frac{\lambda_2 \lambda_3 m_{12}^2}{16\pi^2 |m_{12}^2|}. \quad (3.17)$$

However, the Higgs potential still remains CP-invariant, due to the fulfillment of the following conditions [43]:

$$\text{Im}(m_{12}^4 \lambda_5^*) = \text{Im}(m_{12}^2 \lambda_6^*) = \text{Im}(m_{12}^2 \lambda_7^*) = 0. \quad (3.18)$$

Therefore, there is no 'CP-crisis' arising from large contributions to electric dipole moments in the MS-2HDM, unlike in the case of MSSM.

4 Misalignment predictions

As discussed in section 3, a realistic Higgs spectrum can be obtained by softly breaking the maximal SO(5) symmetry of the 2HDM potential at some high scale μ_X by considering $\text{Re}(m_{12}^2) \neq 0$. As a consequence, there will be some deviation from the alignment limit in

---

[8]In Type-I 2HDM, there exists an additional possibility of realizing an exact Z_2 symmetry [33] which leads to an exact alignment, i.e. in the context of the so-called inert 2HDM [49].

the low-energy Higgs spectrum. By requiring that the mass and couplings of the SM-like Higgs boson in our MS-2HDM are consistent with the latest Higgs data from the LHC [3, 4, 50], we can derive predictions for the remaining scalar spectrum and compare them with the existing (in)direct limits on the heavy Higgs sector. Our subsequent numerical results are derived for the Type-II 2HDM scenario, but the analysis could be easily extended to other 2HDM scenarios.

For the SM-like Higgs boson mass, we will use the 3σ allowed range from the recent CMS and ATLAS Higgs mass measurements [4, 50]:

$$M_H \in \begin{bmatrix} 124.1, & 126.6 \end{bmatrix} \text{ GeV} . \tag{4.1}$$

For the Higgs couplings to the SM vector bosons and fermions, we use the constraints in the $(\tan\beta, \ \beta - \alpha)$ plane derived from a recent global fit for the Type-II 2HDM [21, 22].[9] For a given set of SO(5) boundary conditions $\{\mu_X, \tan\beta(\mu_X), \lambda(\mu_X)\}$, we thus require that the RG-evolved 2HDM parameters at the weak scale must satisfy the above constraints on the lightest CP-even Higgs boson sector. This requirement of *alignment* with the SM Higgs sector puts stringent constraints on the MS-2HDM parameter space, as shown in figure 2. Here the solid, dashed, and dotted blue shaded regions respectively show the 1σ, 2σ and 3σ excluded regions due to misalignment of the mixing angle α from its allowed range derived from the global fit. The shaded red region is theoretically inaccessible, as there is no viable solution to the RGEs in this area. We ensure that the remaining allowed (white) region satisfies the necessary theoretical constraints, i.e. positivity and vacuum stability of the Higgs potential, and perturbativity of the Higgs self-couplings [6]. From figure 2, we find that there exists an upper limit of $\mu_X \lesssim 10^9 \text{ GeV}$ on the SO(5)-breaking scale of the 2HDM potential, beyond which an ultraviolet completion of the theory must be invoked. Moreover, for $10^5 \text{ GeV} \lesssim \mu_X \lesssim 10^9 \text{ GeV}$, only a narrow range of $\tan\beta$ values are allowed.

For the allowed parameter space of our MS-2HDM as shown in figure 2, we obtain concrete predictions for the remaining Higgs spectrum. In particular, the alignment condition imposes a *lower* bound on the soft breaking parameter $\text{Re}(m_{12}^2)$, and hence, on the heavy Higgs spectrum. We compare this limit with the existing experimental limits on the heavy Higgs sector of the 2HDM [40], and find that the alignment limits obtained here are more stringent in a wide range of the parameter space. The most severe experimental constraint comes from the charged Higgs sector, which give significant contributions to various flavour observables, e.g. $B \to X_s\gamma$ [51–54]. For this, we use the global fit results for the Type-II 2HDM from [21], which includes limits derived from electroweak precision data, as well as flavour constraints from Δm_{B_s} and $B \to X_s\gamma$ relevant for the low $\tan\beta$ region. The comparison of the existing limit on the charged Higgs-boson mass as a function of $\tan\beta$ with our predicted limits from the alignment condition for a typical value of the boundary scale $\mu_X = 3 \times 10^4 \text{ GeV}$ is shown in figure 3. It is clear that the alignment limits are stronger than the indirect limits, except in the very small and very large $\tan\beta$ regimes. For $\tan\beta \lesssim 1$ region, the indirect limit obtained from the $Z \to b\bar{b}$ precision observable

---

[9]Note that in our convention, the couplings of the SM-like Higgs boson to vector bosons is proportional to $\cos(\beta - \alpha)$ [cf. (A.8)]. Hence, the natural alignment limit is obtained for $\alpha = \beta$, and *not* for $\alpha = \beta - \pi/2$, as conventionally used in literature.
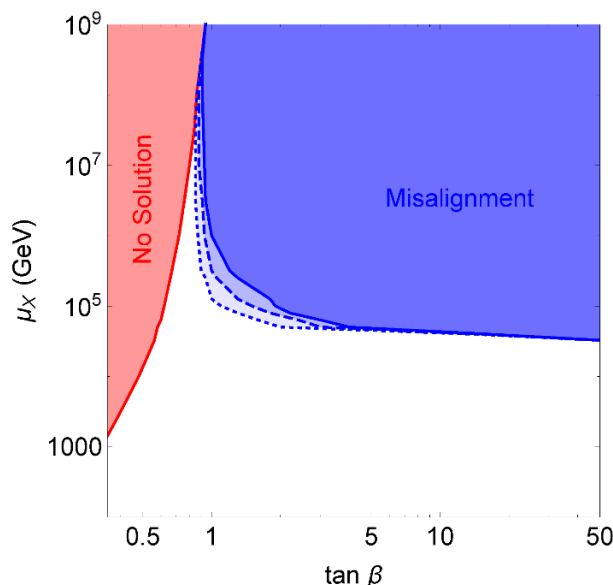
Figure 2. Alignment constraints in the $(\tan\beta, \mu_X)$-plane of the maximally symmetric Type-II 2HDM. The blue shaded regions show the 1σ (dotted), 2σ (dashed) and 3σ (solid) exclusion regions from the alignment condition. The red shaded region is theoretically excluded in this model.

becomes the strictest [21, 55]. Similarly, for the large $\tan\beta \gtrsim 30$ case, the alignment limit can be easily obtained [cf. (3.7)] without requiring a large soft-breaking parameter m_{12}^2, and therefore, the lower limit on the charged Higgs mass derived from the misalignment condition becomes somewhat weaker in this regime.

From figure 2, it should be noted that for $\mu_X \gtrsim 10^5$ GeV, phenomenologically acceptable alignment is not possible in the MS-2HDM for large $\tan\beta$ *and* large m_{12}^2, while keeping the lightest CP-even Higgs boson within the experimentally allowed range (4.1) and maintaining vacuum stability up to the scale μ_X. Therefore, $\mu_X \gtrsim 10^5$ GeV also leads to an *upper* bound on the charged Higgs-boson mass $M_{h^\pm}$ from the misalignment condition, depending on $\tan\beta$. This is illustrated in figure 4 for $\mu_X = 10^5$ GeV. Here the green shaded regions show the 1σ (dotted), 2σ (dashed) and 3σ (solid) *allowed* regions, whereas the corresponding red shaded regions are the experimentally exclusion regions at 1σ (dotted), 2σ (dashed) and 3σ (solid). On the other hand, for $\mu_X \lesssim 10^5$ GeV, a phenomenologically acceptable aligned solution with an arbitrarily large m_{12}^2 is allowed for any value of $\tan\beta$ [cf. figure 2], and hence in this case, there exists only a lower limit on $M_{h^\pm}$, as shown by the blue shaded (exclusion) regions in figure 3.

Similar alignment constraints are obtained for the heavy neutral pseudo-Goldstone bosons h and a, which are predicted to be quasi-degenerate with the charged Higgs boson $h^\pm$ in the MS-2HDM [cf. (3.2)]. The current experimental lower limits on the heavy neutral Higgs sector [40] are much weaker than the alignment constraints in this case. Thus, the MS-2HDM scenario provides a natural reason for the absence of a heavy Higgs signal below the top-quark threshold, and this has important consequences for the non-standard Higgs searches in the run-II phase of the LHC, as discussed in the following section.
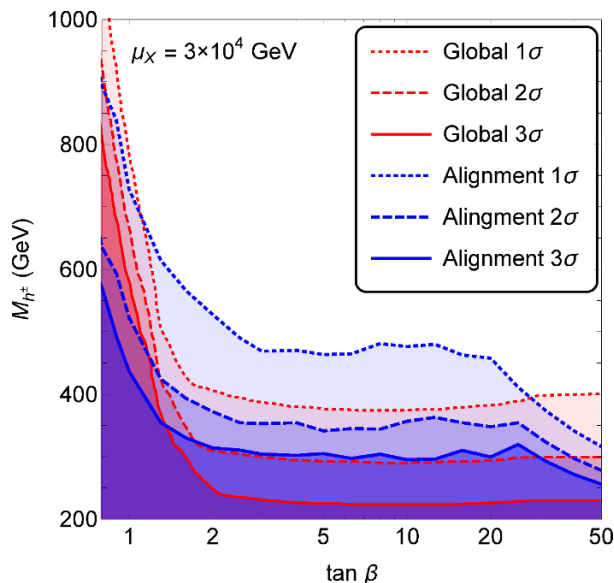
Figure 3. The 1σ (dotted), 2σ (dashed) and 3σ (solid) lower limits on the charged Higgs mass obtained from the alignment condition (blue lines) in the maximally symmetric Type-II 2HDM with $\mu_X = 3 \times 10^4$ GeV. For comparison, the corresponding lower limits from a global fit are also shown (red lines).
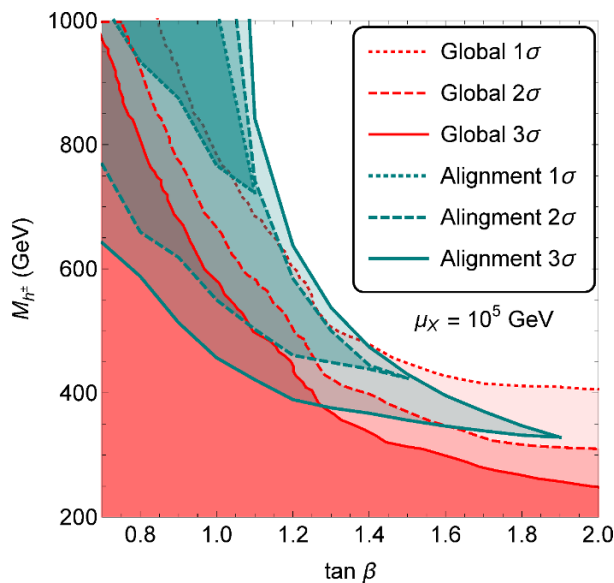
Figure 4. Alignment limits on the charged Higgs mass $M_{h^\pm}$ in the maximally symmetric Type-II 2HDM with $\mu_X = 10^5$ GeV. The dark green regions show the 1σ (dotted), 2σ (dashed) and 3σ (solid) regions *allowed* by alignment constraints in the model. The existing lower limits from a global fit are also shown (red lines) for comparison.

5   Collider signals

In the alignment limit, the couplings of the lightest CP-even Higgs boson are exactly similar to the SM Higgs couplings, while the heavy CP-even Higgs boson preferentially couples to fermions (see appendix A). Therefore, two of the relevant Higgs production mechanisms at the LHC, namely, the vector boson fusion and Higgstrahlung processes are suppressed for the gaugephobic heavy neutral Higgs sector. As a consequence, the only relevant production channels to probe the neutral Higgs sector of the MS-2HDM are the gluon-gluon fusion and $t\bar{t}h$ ($b\bar{b}h$) associated production mechanisms at low (high) $\tan\beta$. For the charged Higgs sector of the MS-2HDM, the dominant production mode is the associated production process: $gg \to \bar{t}bh^+ + t\bar{b}h^-$, irrespective of $\tan\beta$.

5.1   Branching fractions

For our collider analysis, we calculate all the branching ratios of the heavy Higgs sector in the MS-2HDM as a function of their masses using the public C++ code 2HDMC [56, 57]. The results for $\tan\beta = 2$ and with SO(5)-symmetric boundary conditions at $\mu_X = 3 \times 10^4$ GeV are shown in figure 5 for illustration. It is clear that for the heavy neutral Higgs bosons, the $t\bar{t}$ decay mode is the dominant one over most of the MS-2HDM parameter space. However, this is true only for low $\tan\beta \lesssim 5$, since as we go to higher $\tan\beta$ values, the $b\bar{b}$ decay mode becomes dominant, with a sub-dominant contribution from $\tau^+\tau^-$, whereas the $t\bar{t}$ mode gets Yukawa suppressed. This is illustrated in figure 6, where we compare BR$(h \to t\bar{t})$, BR$(h \to b\bar{b})$ and BR$(h \to \tau^+\tau^-)$ for three representative values of $\tan\beta = 2$ (solid), 5 (dashed) and 10 (dotted). For the charged Higgs boson $h^{+(-)}$, the $t\bar{b}(\bar{t}b)$ mode is the dominant one over the entire parameter space, as shown in figure 5 for $\tan\beta = 2$, and this is true even for larger $\tan\beta$.

5.2   Charged Higgs signal

The detection of a charged Higgs boson will be an unequivocal evidence for a beyond SM Higgs sector, and in particular, a 'smoking gun' signal for a 2HDM. For $M_{h^\pm} < M_t$, i.e. below the top-quark threshold, stringent collider limits have been set on its production directly through top quark decays $t \to h^+b$, followed by h^+ decays to $\tau^+\nu_\tau$ [58, 59], $\tau^+ +$ jets [60] and $c\bar{s}$ [61, 62]. For charged Higgs boson masses above the top-quark threshold, the $h^+ \to t\bar{b}$ decay channel opens up, and quickly becomes the dominant channel. In fact, in the Type-II 2HDM, the $h^+\bar{t}b$ coupling (A.14) implies that for $M_{h^+} > M_t + M_b$, the branching fraction of $h^+ \to t\bar{b}$ is almost 100% (cf. figure 5), independent of $\tan\beta$. This leads to mostly $t\bar{t}b\bar{b}$ final states at the LHC via

$$gg \;\to\; \bar{t}bh^+ + t\bar{b}h^- \;\to\; t\bar{t}b\bar{b}\,. \tag{5.1}$$

The experimental observation of this channel is challenging due to large QCD backgrounds and the non-trivial event topology, involving at least four b-jets [63]. Nevertheless, we should emphasize here that (5.1) is the most promising channel for the charged Higgs signal in the MS-2HDM, because other interesting possibilities, such as $h^\pm \to aW^\pm, hW^\pm$ [64],
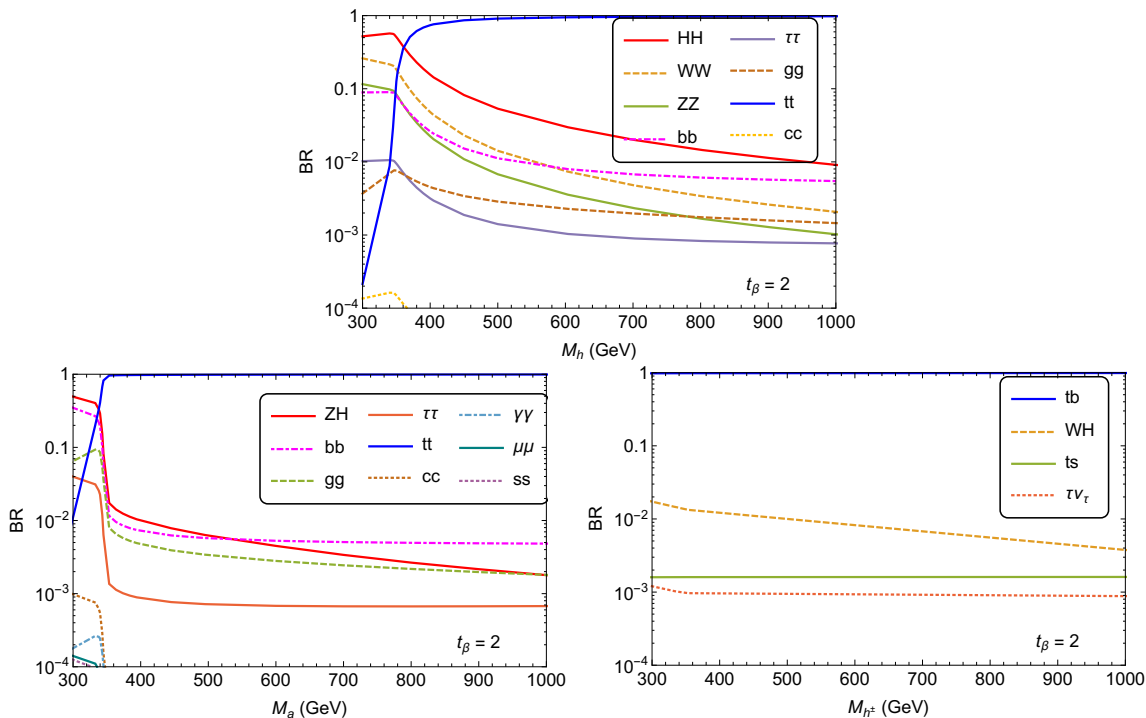
Figure 5. The decay branching ratios of the heavy Higgs bosons in the maximally symmetric Type-II 2HDM for low $\tan\beta$.
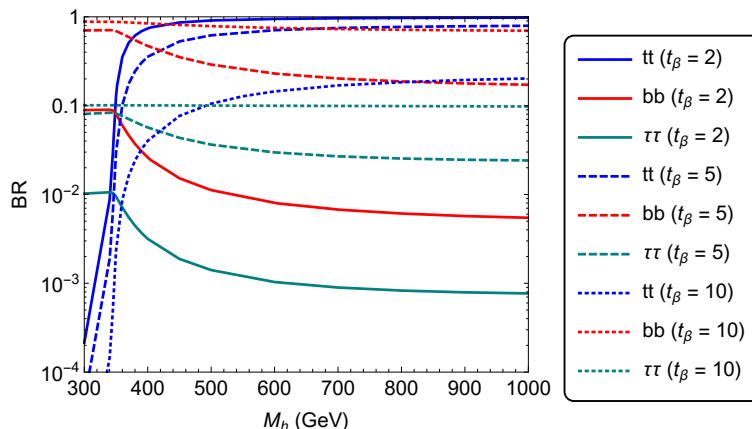
Figure 6. Comparison of $\mathrm{BR}(h \to t\bar{t})$, $\mathrm{BR}(h \to b\bar{b})$ and $\mathrm{BR}(h \to \tau^+\tau^-)$ for different values of $\tan\beta$ in the maximally symmetric Type-II 2HDM.
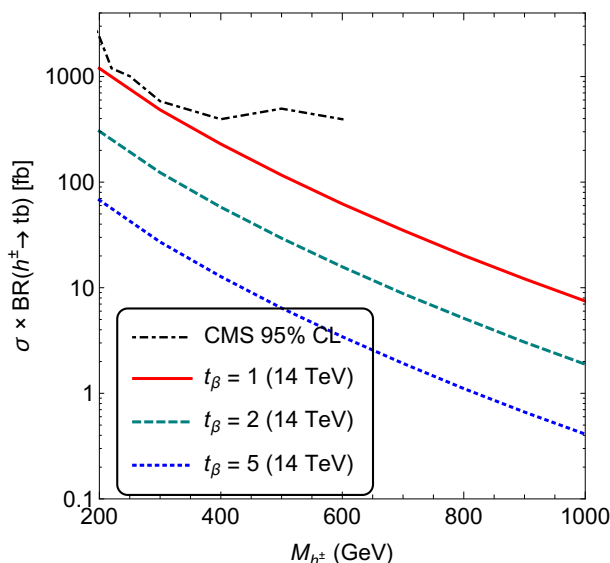
are not open in this scenario due to the kinematical constraints imposed by the quasi-degeneracy of the heavy Higgs sector [cf. (3.2) and figure 1 (left panel)].

A recent CMS study [65] has presented for the first time a realistic analysis of the process (5.1), with the following decay chain:

$$gg \;\to\; h^{\pm} tb \;\to\; (\ell\nu_\ell bb)(\ell'\nu_{\ell'}b)b \tag{5.2}$$

(ℓ, ℓ' beings electrons or muons). Using the $\sqrt{s} = 8\,\mathrm{TeV}$ LHC data, they have derived

Figure 7. Predictions for the cross section of the process (5.1) in the Type-II MS-2HDM at $\sqrt{s} = 14\,\mathrm{TeV}$ LHC for various values of $\tan\beta$. For comparison, we have also shown the current 95% CL CMS upper limit from the $\sqrt{s} = 8\,\mathrm{TeV}$ data [65].

95% CL upper limits on the production cross section $\sigma(gg \to h^{\pm}tb)$ times the branching ratio $\mathrm{BR}(h^{\pm} \to tb)$ as a function of the charged Higgs mass, as shown in figure 7. In the same figure, we show the corresponding predictions at $\sqrt{s} = 14\,\mathrm{TeV}$ LHC in the Type-II MS-2HDM for some representative values of $\tan\beta$. The cross section predictions were obtained at leading order (LO) by implementing the 2HDM in `MadGraph5` [66, 67] and using the `NNPDF2.3` PDF sets [68, 69].[10] A comparison of these cross sections with the CMS limit suggests that the run-II phase of the LHC might be able to probe a portion of the MS-2HDM parameter space using the process (5.1).

In order to make a rough estimate of the $\sqrt{s} = 14\,\mathrm{TeV}$ LHC sensitivity to the charged Higgs signal (5.1) in the MS-2HDM, we perform a parton level simulation of the signal and background events using `MadGraph5_aMC@NLO` [66, 67]. For the event reconstruction, we use some basic selection cuts on the transverse momentum, pseudo-rapidity and dilepton invariant mass, following the recent CMS analysis [65]:

$$
\begin{aligned}
p_T^{\ell} &> 20\,\mathrm{GeV}, \quad |\eta^{\ell}| < 2.5, \quad \Delta R^{\ell\ell} > 0.4, \\
M_{\ell\ell} &> 12\,\mathrm{GeV}, \quad |M_{\ell\ell} - M_Z| > 10\,\mathrm{GeV}, \\
p_T^{j} &> 30\,\mathrm{GeV}, \quad |\eta^{j}| < 2.4, \quad \not{E}_T > 40\,\mathrm{GeV}.
\end{aligned}
\tag{5.3}
$$

Jets are reconstructed using the anti-k_T clustering algorithm [71] with a distance parameter of 0.5. Since four b-jets are expected in the final state, at least two b-tagged jets are required in the signal events, and we assume the b-tagging efficiency for each of them to be 70%.

The inclusive SM cross section for $pp \to t\bar{t}b\bar{b} + X$ is ~ 18 pb at NLO, with roughly 30% uncertainty due to higher order QCD corrections [72]. Most of the QCD background for

---

[10]For an updated and improved next-to-leading order (NLO) calculation, see [70].

the $4b + 2\ell + \not{E}_T$ final state given by (5.2) can be reduced significantly by reconstructing at least one top-quark. As we will show below, the remaining irreducible background due to SM $t\bar{t}b\bar{b}$ production can be suppressed with respect to the signal by reconstructing the charged Higgs boson mass, once a valid signal region is defined, e.g. in terms of an observed excess of events at the LHC in future. For the semi-leptonic decay mode of top-quarks as in (5.2), one cannot directly use an invariant mass observable to infer $M_{h^\pm}$, as both the neutrinos in the final state give rise to missing momentum. A useful quantity in this case is the M_{T2} variable, also known as the 'stransverse mass' [73], defined as

$$ M_{T2} \;=\; \min_{\left\{ \not{\mathbf{p}}_{T_{\mathrm{a}}} + \not{\mathbf{p}}_{T_{\mathrm{b}}} = \not{\mathbf{p}}_T \right\}} \Big[\max \left\{ m_{T_{\mathrm{a}}}, m_{T_{\mathrm{b}}} \right\} \Big] \;, \tag{5.4} $$

where $\{a\}, \{b\}$ stand for the two sets of particles in the final state, each containing a neutrino with part of the missing transverse momentum ($\not{\mathbf{p}}_{T_{\mathrm{a,b}}}$). Minimization over all possible sums of these two momenta gives the observed missing transverse momentum $\not{\mathbf{p}}_T$, whose magnitude is the same as $\not{E}_T$ in our specific case. In (5.4), m_{T_i} (with $i =$a,b) is the usual transverse mass variable for the system $\{i\}$, defined as

$$ m_{T_i}^2 \;=\; \left(\sum_{\mathrm{visible}} E_{T_i} + \not{E}_{T_i} \right)^2 - \left(\sum_{\mathrm{visible}} \mathbf{p}_{T_i} + \not{\mathbf{p}}_{T_i} \right)^2 \;. \tag{5.5} $$

For the correct combination of the final state particles in (5.2), i.e. for $\{a\} = (\ell \nu_\ell bb)$ and $\{b\} = (\ell' \nu_{\ell'} bb)$ in (5.4), the maximum value of M_{T2} represents the charged Higgs boson mass, with the M_{T2} distribution smoothly dropping to zero at this point. This is illustrated in figure 8 (left panel) for a typical choice of $M_{h^\pm} = 300\,\mathrm{GeV}$. For comparison, we also show the M_{T2} distribution for the SM background, which obviously does not have a sharp endpoint. Thus, for a given hypothesized signal region defined in terms of an excess due to $M_{h^\pm}$, we may impose an additional cut on $M_{T2} \leq M_{h^\pm}$ to enhance the signal (5.2) over the irreducible SM background.

Apart from the decay chain (5.2) as considered in the CMS analysis [65], we also examine another decay chain involving hadronic decay modes of the secondary top-quark from the charged Higgs decay, i.e.

$$ gg \;\to\; h^\pm tb \;\to\; (jjbb)(\ell \nu_\ell b)b \;. \tag{5.6} $$

In this case, the charged Higgs boson mass can be reconstructed using the invariant mass M_{jjbb} for the correct combination of the b-quark jets. This is illustrated in figure 8 (right panel) for $M_{h^\pm} = 300\,\mathrm{GeV}$, along with the expected SM background. Thus, for the decay chain (5.6), one can use an invariant mass cut of M_{jjbb} around $M_{h^\pm}$ to observe the signal over the irreducible SM background. Note that the hadronic mode (5.6) has a larger branching ratio, although from the experimental point of view, one has to deal with the uncertainties in the jet energy measurements, combinatorics and the resulting uncertainties in the invariant mass reconstruction of multiparticle final states.

Thus, in principle, we can obtain an observable charged Higgs signal in the MS-2HDM above the irreducible SM background by using one of the methods shown in figure 8 to
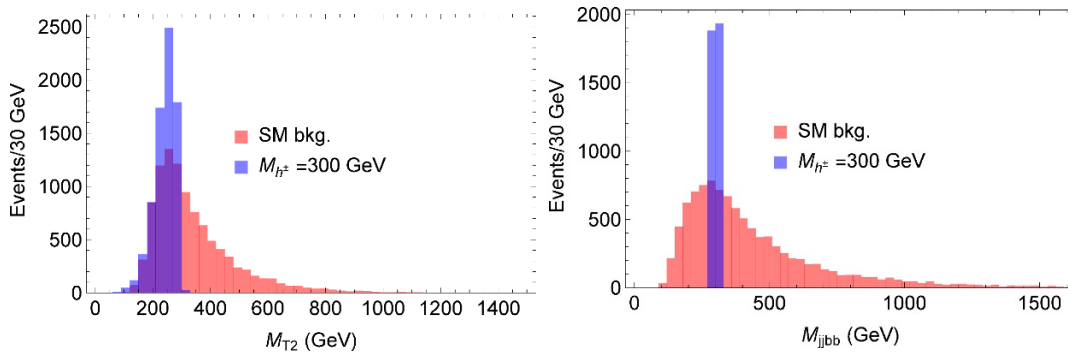
Figure 8. An illustration of the charged Higgs boson mass reconstruction using the M_{T2} (left panel) and invariant mass (right panel) observables. The irreducible SM background distribution is also shown for comparison.

reconstruct efficiently the charged Higgs boson mass. Assuming this, we present an estimate of the signal to background ratio for the charged Higgs signal given by (5.1) at $\sqrt{s} = 14\,\mathrm{TeV}$ LHC with $300\,\mathrm{fb}^{-1}$ for some typical values of $\tan\beta$ in figure 9. Since the mass of the charged Higgs boson is a priori unknown, we vary the charged Higgs mass, and for each value of $M_{h^\pm}$, we assume that it can be reconstructed around its actual value within $30\,\mathrm{GeV}$ uncertainty. We believe such a mass resolution is possible experimentally, given the fact that the width of the charged Higgs boson $\Gamma_{h^\pm}$ in the mass range shown in figure 9 is always smaller than the chosen mass uncertainty.[11] From figure 9, we see that the $t\bar{t}b\bar{b}$ channel (5.1) is effective for charged Higgs searches at the LHC for low $\tan\beta$ values. Note that the production cross section $\sigma(gg \to \bar{t}bh^+)$ decreases rapidly with increasing $\tan\beta$ due to the Yukawa suppression [cf. (A.14)], even though the branching fraction of $h^+ \to \bar{t}b$ remains close to 100%.

5.3 Heavy neutral Higgs signal

Since the heavy CP-even Higgs boson in the MS-2HDM is gaugephobic, most of the existing collider limits derived using the decay modes $h \to WW$ [74, 75] and $h \to ZZ$ [76] do not apply in this case. The only existing searches relevant to the heavy CP-even sector of the MS-2HDM scenario are those based on $gg \to h \to \tau^+\tau^-$ and $gg \to b\bar{b}h \to b\bar{b}\tau^+\tau^-$ [77, 78]. However, due to the relatively small branching ratio of $h \to \tau^+\tau^-$, the model-independent upper limits derived in [77, 78] are easily satisfied for the heavy Higgs spectrum presented here. Similarly, the $h \to \gamma\gamma$ branching ratio in the MS-2HDM is $\sim 10^2 - 10^3$ times smaller than that for the SM Higgs boson; therefore, the cross section limits derived from the $\gamma\gamma$ channel [79, 80] are also easily satisfied. So far there have been no direct searches for heavy neutral Higgs bosons involving $t\bar{t}$ and/or $b\bar{b}$ final states, mainly due to the challenges associated with uncertainties in the jet energy scales and the combinatorics arising from complicated multiparticle final states in a busy QCD environment. Nevertheless, these channels become pronounced in the MS-2HDM scenario, and hence, we will make here a preliminary attempt to study them.

---

[11] For instance, for $\tan\beta = 2$, $\Gamma_{h^\pm} = 1.9\,\mathrm{GeV}$ at $M_{h^\pm} = 300\,\mathrm{GeV}$ and $\Gamma_{h^\pm} = 22\,\mathrm{GeV}$ at $M_{h^\pm} = 2\,\mathrm{TeV}$.
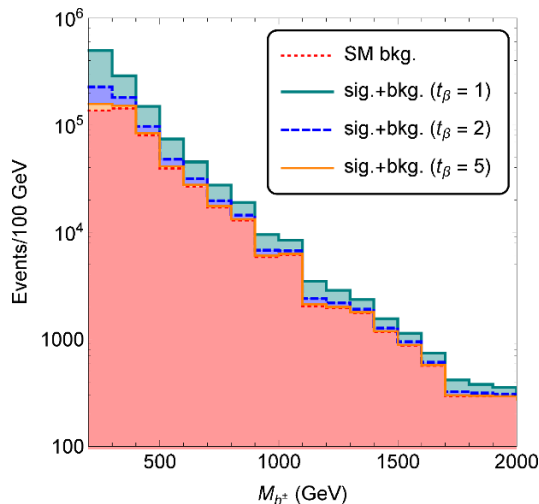
Figure 9. Predicted number of events for the $t\bar{t}b\bar{b}$ signal from the charged pseudo-Goldstone boson in the MS-2HDM at $\sqrt{s} = 14\,\text{TeV}$ LHC with 300 fb^{-1} integrated luminosity. The results are shown for three different values of $\tan\beta$ =1 (green solid), 2 (blue dashed) and 5 (orange solid). The irreducible SM background (red dotted) is controlled by assuming an efficient mass reconstruction technique, as described in the text.

It is worth mentioning here that the Higgs pair production process $pp \to h \to HH$ (see e.g. [81]) is another interesting possibility. However, as shown in (A.12), the $h \to HH$ decay mode should also vanish in the exact alignment limit $\alpha \to \beta$, just like the $h \to VV$ decay modes. Therefore, the LHC limits derived using the $h \to HH$ channel [82, 83] are applicable only below the top threshold $M_h \leq 2M_t$ in the MS-2HDM (cf. figure 5). On the other hand, the lower limits on the heavy Higgs sector, as derived in section 4 (e.g. figures 3 and 4) strongly suggest a mass spectrum above the $t\bar{t}$ threshold, where the $h \to HH$ branching fraction drops orders of magnitude below that of $h \to t\bar{t}$ ($b\bar{b}$) at low (high) $\tan\beta$.

In light of the above discussion, we propose a new search channel for the heavy neutral Higgs boson in the MS-2HDM via the $t\bar{t}t\bar{t}$ final state:

$$gg \;\to\; t\bar{t}h \;\to\; t\bar{t}t\bar{t}\,. \tag{5.7}$$

Such four top final states have been proposed before in the context of other exotic searches at the LHC, e.g. composite top [84–86], low-scale extra-dimensions [87, 88] and SUSY with light stops and gluinos [89]. However, their relevance for heavy Higgs searches have not been explored so far. We note here that the existing 95% CL experimental upper limit on the four top production cross section is 59 fb from ATLAS [90] and 32 fb from CMS [91], whereas the SM prediction for the inclusive cross section of the process $pp \to t\bar{t}t\bar{t} + X$ is about 10-15 fb [92].

To get a rough estimate of the signal to background ratio for our new four-top signal, we perform a parton-level simulation of the signal and background events at LO in QCD using `MadGraph5_aMC@NLO` [66, 67] with `NNPDF2.3` PDF sets [68, 69]. For the inclusive
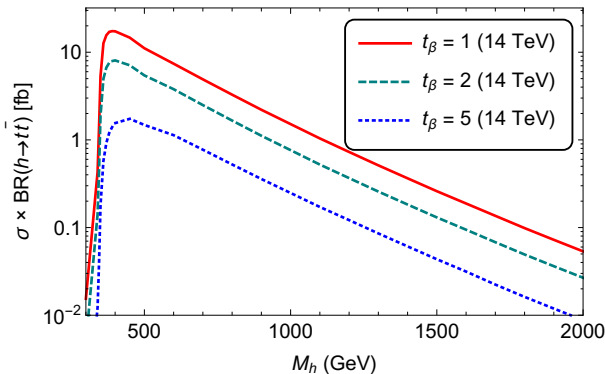
Figure 10. Predictions for the cross section of the process (5.7) in the Type-II MS-2HDM at $\sqrt{s} = 14\,\mathrm{TeV}$ LHC for various values of $\tan\beta$.

SM cross section for the four-top final state at $\sqrt{s} = 14\,\mathrm{TeV}$ LHC, we obtain $11.85\,\mathrm{fb}$, whereas our proposed four-top signal cross sections are found to be comparable or smaller depending on M_h and $\tan\beta$, as shown in figure 10. However, since we expect one of the $t\bar{t}$ pairs coming from an on-shell h decay to have an invariant mass around M_h, we can use this information to significantly boost the signal over the irreducible SM background. Note that all the predicted cross sections shown in figure 10 are well below the current experimental upper bound [91].

Depending on the W decay mode from $t \to Wb$, there are 35 final states for four top decays. According to a recent ATLAS analysis [93], the experimentally favoured channel is the semi-leptonic/hadronic final state with two same-sign isolated leptons. Although the branching fraction for this topology (4.19%) is smaller than most of the other channels, the presence of two same-sign leptons in the final state allows us to reduce the large QCD background substantially, including that due to the SM production of $t\bar{t}b\bar{b}$+jets.[12] Therefore, we will only consider the following decay chain in our preliminary analysis:

$$gg \;\to\; t\bar{t}h \;\to\; (t\bar{t})(t\bar{t}) \;\to\; \Big((\ell^{\pm}\nu_{\ell}b)(jjb)\Big)\Big((\ell'^{\pm}\nu_{\ell'}b)(jjb)\Big). \tag{5.8}$$

For event reconstruction, we will use the same selection cuts as in (5.3), and in addition, following [93], we require the scalar sum of the p_T of all leptons and jets (defined as H_T) to exceed 350 GeV.

As in the charged Higgs boson case [cf. (5.2)], the heavy Higgs mass can be reconstructed from the signal given by (5.8) using the M_{T2} endpoint technique. The correct combination of visible final states in (5.8) will lead to a smooth drop at M_h in the M_{T2} distribution, as illustrated in figure 11 for a typical choice of $M_h = 450\,\mathrm{GeV}$. As shown in the same figure, the SM background does not exhibit such a feature, and hence, an additional selection cut on $M_{T2} \leq M_h$ can be used to enhance the signal to background ratio in the signal region.

Our simulation results for the predicted number of signal and background events for the process (5.8) at $\sqrt{s} = 14\,\mathrm{TeV}$ LHC with $300\,\mathrm{fb}^{-1}$ luminosity are shown in figure 12.

---

[12]For a detailed analysis of the reducible and irreducible four top background, see [93].
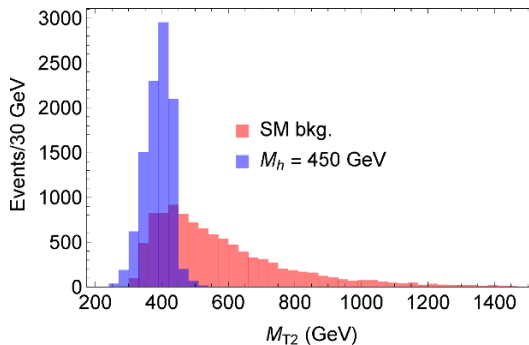
Figure 11. An illustration of the heavy CP-even Higgs boson mass reconstruction using M_{T2} observable. The irreducible SM background distribution is also shown for comparison.
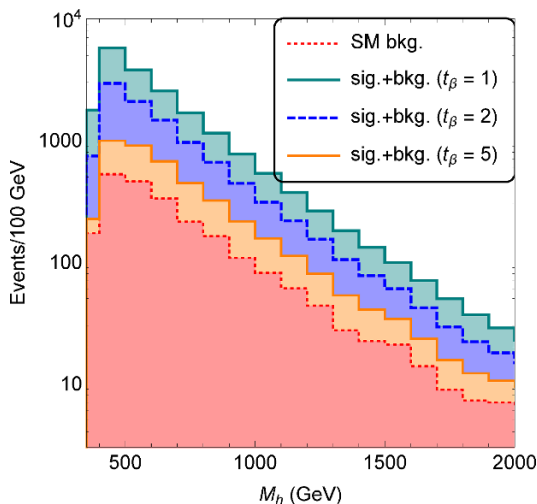
Figure 12. Predicted number of events for the $t\bar{t}t\bar{t}$ signal from the neutral pseudo-Goldstone boson in the MS-2HDM at $\sqrt{s} = 14$ TeV LHC with 300 fb^{-1} integrated luminosity. The results are shown for three different values of $\tan\beta$ =1 (green solid), 2 (blue dashed) and 5 (orange solid). The SM background (red dotted) is controlled by assuming an efficient mass reconstruction technique, as outlined in the text.

The signal events are shown for three representative values of $\tan\beta$. Here we vary the a priori unknown heavy Higgs mass, and for each value of M_h, we assume that it can be reconstructed around its actual value within 30 GeV uncertainty, which should be feasible experimentally, given the fact that the decay width of h is always smaller the chosen mass uncertainty window for the entire mass range shown in figure 12. From this preliminary analysis, we find that the $t\bar{t}t\bar{t}$ channel provides the most promising collider signal to probe the heavy Higgs sector in the MS-2HDM at low values of $\tan\beta \lesssim 5$.

The above analysis is also applicable for the CP-odd Higgs boson a, which has similar production cross sections and $t\bar{t}$ branching fractions as the CP-even Higgs h. However, the $t\bar{t}h(a)$ production cross section as well as the $h(a) \to t\bar{t}$ branching ratio decreases with increasing $\tan\beta$. This is due to the fact that the $ht\bar{t}$ coupling in the alignment limit is $\cos\alpha/\sin\beta \sim \cot\beta$, which is same as the $at\bar{t}$ coupling [cf. (A.13)]. Thus, the high

$\tan\beta$ region of the MS-2HDM cannot be searched via the $t\bar{t}t\bar{t}$ channel proposed above, and one needs to consider the channels involving down-sector Yukawa couplings, e.g. $b\bar{b}b\bar{b}$ and $b\bar{b}\tau^+\tau^-$, which are very challenging in the LHC environment [63]. For instance, the SM $b\bar{b}b\bar{b}$ cross section at $\sqrt{s} = 14\,\mathrm{TeV}$ LHC is about 140 pb at NLO [94], whereas the $pp \to b\bar{b}h \to b\bar{b}b\bar{b}$ signal cross section for $M_h = 300\,\mathrm{GeV}$ and $\tan\beta = 10$ is only about 0.3 pb at NLO, as estimated using the public FORTRAN code SusHi [95, 96]. In practice, one would require a sophisticated jet substructure technique [97, 98] to disentangle such a tiny signal from the huge QCD background. It is also worth commenting here that the simpler process $pp \to h \to t\bar{t}\ (b\bar{b})$ at low (high) $\tan\beta$ similarly suffers from a huge SM $t\bar{t}\ (b\bar{b})$ QCD background, even after imposing an $M_{t\bar{t}\ (b\bar{b})}$ cut.

Before concluding this section, we should clarify that although we were able to obtain a sizeable signal-to-background ratio in the low $\tan\beta$ regime for the signals (5.2), (5.6) and (5.8) using efficient mass reconstruction techniques in the signal region, as described in the subsections 5.2 and 5.3 above, these results are valid only at the parton level. In a realistic detector environment, the sharp features of the signal shown in figures 8 and 11 may not survive, and therefore, the signal-to-background ratio might get somewhat reduced than that shown here. However, a detailed realistic detector-level analysis of these signals in our MS-2HDM scenario, including realistic top reconstruction efficiencies and smearing effects, is beyond the scope and main focus of this article, and is being pursued in a separate dedicated study.

6 Conclusions

We have analyzed the symmetries of the 2HDM scalar potential to naturally justify the so-called SM alignment limit, independently of the heavy Higgs spectrum and the value of $\tan\beta$. We show that in the Type-II 2HDM, there exist *only* three different symmetry realizations, cf. (2.8), (3.15) and (3.16), which could lead to a natural alignment by satisfying (3.8) for *any* value of $\tan\beta$. In the context of the Maximally Symmetric Two Higgs Doublet Model based on the SO(5) group, we demonstrate how small deviations from this alignment limit are naturally induced by RG effects due to the hypercharge gauge coupling g' and third generation Yukawa couplings, which also break the custodial symmetry of the theory. In addition, a non-zero soft SO(5)-breaking mass parameter is required to yield a viable Higgs spectrum consistent with the existing experimental constraints. Employing the current Higgs signal strength data from the LHC, which disfavour large deviations from the alignment limit, we derive important constraints on the 2HDM parameter space. In particular, we predict lower limits on the heavy Higgs spectrum, which prevail the present limits in a wide range of parameter space. Depending on the scale where the maximal symmetry could be realized in nature, we also obtain an upper limit on the heavy Higgs masses in certain cases, which could be completely probed during the run-II phase of the LHC. Finally, we propose a new collider signal with four top quarks in the final state, which can become a valuable observational tool to directly probe the heavy Higgs sector of the 2HDM in the SM alignment limit for low values of $\tan\beta$. It would be interesting to investigate how this tool could be applied to supersymmetric theories in the alignment limit.

Acknowledgments

A Higgs spectrum and couplings in a general 2HDM

Here we will restrict our discussion to 2HDM potentials realizing CP-conserving vacua. In this case, the minimization of a CP-conserving 2HDM potential (1.2) yields the following real non-negative vacuum expectation values (VEVs):

$$\langle \Phi_1 \rangle \;=\; \frac{1}{\sqrt{2}} \begin{pmatrix} 0 \\ v_1 \end{pmatrix}, \qquad \langle \Phi_2 \rangle \;=\; \frac{1}{\sqrt{2}} \begin{pmatrix} 0 \\ v_2 \end{pmatrix}, \tag{A.1}$$

where $v = \sqrt{v_1^2 + v_2^2} = 246.2\,\mathrm{GeV}$ is the SM electroweak VEV and for later convenience, we define $\tan\beta \equiv v_2/v_1$. The two scalar doublets can be expanded in terms of eight real scalar fields as follows:

$$\Phi_j \;=\; \begin{pmatrix} \phi_j^+ \\ \frac{1}{\sqrt{2}}(v_j + \phi_j + i a_j) \end{pmatrix}, \tag{A.2}$$

with $j = 1, 2$. After spontaneous symmetry breaking, there are three Goldstone modes $(G^{\pm}, G^0)$, which become the longitudinal components of the SM $W^{\pm}$ and Z bosons. Thus, there are five remaining physical scalar mass eigenstates: two CP-even (h, H), one CP-odd (a) and two charged $(h^{\pm})$ scalars. The mixing in the CP-odd and charged sectors is governed by the angle β defined above:

$$\begin{pmatrix} G^{\pm} \\ h^{\pm} \end{pmatrix} = \begin{pmatrix} c_\beta & s_\beta \\ -s_\beta & c_\beta \end{pmatrix} \begin{pmatrix} \phi_1^{\pm} \\ \phi_2^{\pm} \end{pmatrix},$$
$$\begin{pmatrix} G^0 \\ a \end{pmatrix} = \begin{pmatrix} c_\beta & s_\beta \\ -s_\beta & c_\beta \end{pmatrix} \begin{pmatrix} a_1 \\ a_2 \end{pmatrix}, \tag{A.3}$$

where $c_\beta \equiv \cos\beta$, $s_\beta \equiv \sin\beta$. On the other hand, in the CP-even sector, we have a new mixing angle α:

$$\begin{pmatrix} H \\ h \end{pmatrix} = \begin{pmatrix} c_\alpha & s_\alpha \\ -s_\alpha & c_\alpha \end{pmatrix} \begin{pmatrix} \phi_1 \\ \phi_2 \end{pmatrix}. \tag{A.4}$$

The corresponding physical mass eigenvalues are given by [42, 43]

$$
\begin{aligned}
M_{h^\pm}^2 &= \frac{m_{12}^2}{s_\beta c_\beta} - \frac{v^2}{2}\left(\lambda_4 + \lambda_5\right) + \frac{v^2}{2 s_\beta c_\beta}\left(\lambda_6 c_\beta^2 + \lambda_7 s_\beta^2\right), \\
M_a^2 &= M_{h^\pm}^2 + \frac{v^2}{2}\left(\lambda_4 - \lambda_5\right), \\
M_H^2 &= \frac{1}{2}\left[(A+B) - \sqrt{(A-B)^2 + 4C^2}\right], \\
M_h^2 &= \frac{1}{2}\left[(A+B) + \sqrt{(A-B)^2 + 4C^2}\right],
\end{aligned}
\tag{A.5}
$$

where we have defined $\tan 2\alpha = 2C/(A-B)$, and

$$
\begin{aligned}
A &= M_a^2 s_\beta^2 + v^2\left(2\lambda_1 c_\beta^2 + \lambda_5 s_\beta^2 + 2\lambda_6 s_\beta c_\beta\right), \\
B &= M_a^2 c_\beta^2 + v^2\left(2\lambda_2 s_\beta^2 + \lambda_5 c_\beta^2 + 2\lambda_7 s_\beta c_\beta\right), \\
C &= -M_a^2 s_\beta c_\beta + v^2\left(\lambda_{34} s_\beta c_\beta + \lambda_6 c_\beta^2 + \lambda_7 s_\beta^2\right).
\end{aligned}
\tag{A.6}
$$

with $\lambda_{34} = \lambda_3 + \lambda_4$. The SM Higgs field is given by

$$
H_{\rm SM} = \phi_1 \cos\beta + \phi_2 \sin\beta = H\cos(\beta-\alpha) + h\sin(\beta-\alpha). \tag{A.7}
$$

From (A.7), the couplings of h and H to the gauge bosons ($V = W^\pm, Z$) with respect to the SM Higgs couplings $g_{H_{\rm SM}VV}$ are given by

$$
g_{hVV} = s_{\beta-\alpha}, \qquad g_{HVV} = c_{\beta-\alpha}. \tag{A.8}
$$

Similarly, unitarity constraints uniquely fix the other Higgs-Higgs-V couplings [5]:

$$
\begin{aligned}
g_{haZ} &= \frac{g}{2\cos\theta_w} c_{\beta-\alpha}, \qquad g_{HaZ} = \frac{g}{2\cos\theta_w} s_{\beta-\alpha}, \\
g_{h^+ h W^-} &= \frac{g}{2} c_{\beta-\alpha}, \quad g_{h^+ H W^-} = \frac{g}{2} s_{\beta-\alpha}, \quad g_{ah^\pm W^\mp} = \frac{g}{2},
\end{aligned}
\tag{A.9}
$$

(where θ_w is the weak mixing angle) in order to satisfy the sum rules [99]

$$
g_{haZ}^2 + g_{HaZ}^2 = \frac{1}{\cos^2\theta_w}(g_{h^+ h W^-}^2 + g_{h^+ H W^-}^2) = \frac{1}{4M_Z^2} g_{H_{\rm SM}ZZ}^2, \tag{A.10}
$$

$$
g_{h^+ h W^-}^2 + g_{h^+ H W^-}^2 = g_{ah^\pm W^\mp}^2 = \frac{1}{4M_W^2} g_{H_{\rm SM}W^+ W^-}^2. \tag{A.11}
$$

For our subsequent discussion, we also write down the h-H-H coupling [24]:

$$
\begin{aligned}
g_{hHH} = \frac{s_{\beta-\alpha}}{4v s_\beta c_\beta}\Big[&2(M_h^2 + 2M_H^2)s_{2\alpha} - 2(M_a^2 + v^2\lambda_5)(s_{2\beta} + 3s_{2\alpha}) \\
&- v^2(\lambda_6 - \lambda_7)(c_{2\beta} + 3c_{2\alpha}) - v^2(\lambda_6 + \lambda_7)(1 + 3c_{2(\beta-\alpha)})\Big].
\end{aligned}
\tag{A.12}
$$

Note that the coupling g_{hHH} is proportional to $s_{\beta-\alpha}$ and so vanishes identically in the alignment limit $\alpha \to \beta$.

To obtain a phenomenologically acceptable theory, we need to forbid Higgs interactions with tree-level FCNCs. This can be accomplished minimally by imposing appropriate

discrete Z_2 symmetries, which will explicitly break in general the custodial symmetries of the theory. By convention, we may take u_R to couple to Φ_2, i.e. $h_1^u = 0$, and then Φ_1 (Φ_2) to couple to d_R, with $h_2^d = 0$ ($h_1^d = 0$), in a Type-II (Type-I) realization of the 2HDM. As our interest is in the Type-II 2HDM, we only list the Yukawa couplings of the neutral scalars with respect to those of $H_{\rm SM}$ for this class of models [5]:

$$
\begin{aligned}
g_{ht\bar{t}} &= \cos\alpha/\sin\beta\,, & g_{hb\bar{b}} &= -\sin\alpha/\cos\beta\,, \\
g_{Ht\bar{t}} &= \sin\alpha/\sin\beta\,, & g_{Hb\bar{b}} &= \cos\alpha/\cos\beta\,, \\
g_{at\bar{t}} &= \cot\beta\,, & g_{ab\bar{b}} &= \tan\beta\,.
\end{aligned}
\tag{A.13}
$$

Finally, we also write down the coupling of the charged scalar to the third-generation quarks [5]:

$$
g_{h^- t\bar{b}} = \frac{g}{2\sqrt{2}M_W}[m_t \cot\beta(1+\gamma_5) + m_b \tan\beta(1-\gamma_5)]\,.
\tag{A.14}
$$

B Two-loop RGEs in a general 2HDM

In this section, we present the two-loop renormalization group equations (RGEs) for the general 2HDM given by (1.2). These results were obtained using the general prescription given in [100–102], as implemented in the public `Mathematica` package `SARAH 4` [103, 104].

The two-loop RGEs for the $SU(3)_c$, $SU(2)_L$ and $U(1)_Y$ gauge couplings are respectively given by

$$
\mathcal{D}g_3 = -\frac{7g_3^3}{16\pi^2} + \frac{g_3^3}{256\pi^4}\left(-26g_3^2 + \frac{9}{2}g_2^2 + \frac{11}{6}g'^2 - 2y_b^2 - 2y_t^2\right)\,,
\tag{B.1}
$$

$$
\mathcal{D}g_2 = -\frac{3g_2^3}{16\pi^2} + \frac{g_2^3}{256\pi^4}\left(12g_3^2 + 8g_2^2 + 2g'^2 - \frac{3}{2}y_b^2 - \frac{3}{2}y_t^2 - \frac{1}{2}y_\tau^2\right)\,,
\tag{B.2}
$$

$$
\mathcal{D}g' = \frac{7g'^3}{16\pi^2} + \frac{g'^3}{256\pi^4}\left(\frac{44}{3}g_3^2 + 6g_2^2 + \frac{104}{9}g'^2 - \frac{5}{6}y_b^2 - \frac{17}{6}y_t^2 - \frac{5}{2}y_\tau^2\right)\,,
\tag{B.3}
$$

where $\mathcal{D} \equiv d/d\ln\mu$ and μ is the usual 't-Hooft mass employed in the regularization of ultraviolet divergences in loop integrals. Note that at the one-loop level, the gauge coupling RGEs do not depend on the Yukawa and scalar couplings, whilst at two loops, they do depend on the quark and lepton Yukawa couplings, for which we have only kept the dominant third-generation contributions.

Similarly for the Yukawa RGEs, we will only consider the third-generation Yukawa couplings, such that for Type-II 2HDM, we have

$$
m_t = \frac{v_2}{\sqrt{2}}h_{2,33}^u \equiv \frac{v_2}{\sqrt{2}}y_t\,, \qquad m_{b(\tau)} = \frac{v_1}{\sqrt{2}}h_{1,33}^{d(e)} \equiv \frac{v_1}{\sqrt{2}}y_{b(\tau)}\,.
\tag{B.4}
$$

With this approximation, the third-generation Yukawa coupling RGEs are given by

$$
\begin{aligned}
\mathcal{D}y_t = {}& \frac{y_t}{16\pi^2}\left(-8g_3^2 - \frac{9}{4}g_2^2 - \frac{17}{12}g'^2 + \frac{9}{2}y_t^2 + \frac{1}{2}y_b^2\right) \\
& + \frac{y_t}{256\pi^4}\left[-108g_3^4 - \frac{21}{4}g_2^4 + \frac{1267}{216}g'^4 + 9g_2^2g_3^2 - \frac{3}{4}g_2^2g'^2 + \frac{19}{9}g_3^2g'^2 + 6\lambda_2^2 + \lambda_3^2 \right.
\end{aligned}
$$

$$
+ \lambda_3\lambda_4 + \lambda_4^2 + \frac{3}{2}(\lambda_5^2 + \lambda_6^2 + 3\lambda_7^2) + \left(\frac{16}{3}g_3^2 + \frac{33}{16}g_2^2 - \frac{41}{144}g'^2 - 2\lambda_3 + 2\lambda_4 \right) y_b^2
$$

$$
+ \left(36g_3^2 + \frac{225}{16}g_2^2 + \frac{131}{16}g'^2 - 12\lambda_2 \right) y_t^2 - \frac{5}{2}y_b^4 - 12y_t^4 - \frac{5}{2}y_b^2 y_t^2 - \frac{3}{4}y_b^2 y_\tau^2 \Bigg], \quad (B.5)
$$

$$
\mathcal{D}y_b = \frac{y_b}{16\pi^2}\left(-8g_3^2 - \frac{9}{4}g_2^2 - \frac{5}{12}g'^2 + \frac{9}{2}y_b^2 + \frac{1}{2}y_t^2 + y_\tau^2 \right)
$$

$$
+ \frac{y_b}{256\pi^4}\Bigg[-108g_3^4 - \frac{21}{4}g_2^4 - \frac{113}{216}g'^4 + 9g_2^2 g_3^2 - \frac{9}{4}g_2^2 g'^2 + \frac{31}{9}g_3^2 g'^2 + 6\lambda_1^2 + \lambda_3^2
$$

$$
+ \lambda_3\lambda_4 + \lambda_4^2 + \frac{3}{2}(\lambda_5^2 + 3\lambda_6^2 + \lambda_7^2) + \left(\frac{16}{3}g_3^2 + \frac{33}{16}g_2^2 - \frac{53}{144}g'^2 - 2\lambda_3 + 2\lambda_4 \right) y_t^2
$$

$$
+ \left(\frac{15}{8}g_2^2 + \frac{25}{8}g'^2 \right) y_\tau^2 + \left(36g_3^2 + \frac{225}{16}g_2^2 + \frac{79}{16}g'^2 - 12\lambda_1 \right) y_b^2
$$

$$
- 12y_b^4 - \frac{9}{4}y_\tau^4 - \frac{5}{2}y_t^4 - \frac{5}{2}y_b^2 y_t^2 - \frac{9}{4}y_b^2 y_\tau^2 \Bigg] , \quad (B.6)
$$

$$
\mathcal{D}y_\tau = \frac{y_\tau}{16\pi^2}\left(-\frac{9}{4}g_2^2 - \frac{15}{4}g'^2 + 3y_b^2 + \frac{5}{2}y_\tau^2 \right)
$$

$$
+ \frac{y_\tau}{256\pi^4}\Bigg[-\frac{21}{4}g_2^4 + \frac{161}{8}g'^4 + \frac{9}{4}g_2^2 g'^2 + 6\lambda_1^2 + \lambda_3^2 + \lambda_3\lambda_4 + \lambda_4^2
$$

$$
+ \frac{3}{2}(\lambda_5^2 + 3\lambda_6^2 + \lambda_7^2) + \left(20g_3^2 + \frac{45}{8}g_2^2 + \frac{25}{24}g'^2 \right) y_b^2
$$

$$
+ \left(\frac{165}{16}g_2^2 + \frac{179}{16}g'^2 - 12\lambda_1 \right) y_\tau^2 - \frac{27}{4}y_b^4 - 3y_\tau^4 - \frac{27}{4}y_b^2 y_\tau^2 - \frac{9}{4}y_b^2 y_t^2 \Bigg] . \quad (B.7)
$$

Similarly, the two-loop RGEs for the VEVs are given by

$$
\mathcal{D}v_1 = \frac{v_1}{16\pi^2}\left[\frac{3}{4}(3g_2^2 + g'^2) - 3y_b^2 - y_\tau^2 \right]
$$

$$
+ \frac{v_1}{256\pi^4}\Bigg[\frac{435}{32}g_2^4 - \frac{149}{32}g'^4 - \frac{3}{16}g_2^2 g'^2 - 6\lambda_1^2 - \lambda_3^2 - \lambda_3\lambda_4 - \lambda_4^2
$$

$$
- \frac{3}{2}(\lambda_5^2 + 3\lambda_6^2 + \lambda_7^2) - \left(20g_3^2 + \frac{45}{8}g_2^2 + \frac{25}{24}g'^2 \right) y_b^2 - \left(\frac{15}{8}g_2^2 + \frac{25}{8}g'^2 \right) y_\tau^2
$$

$$
+ \frac{27}{4}y_b^4 + \frac{9}{4}y_\tau^4 + \frac{9}{4}y_b^2 y_t^2 \Bigg] - \frac{3v_2}{512\pi^4}\Big[(2\lambda_1 + \lambda_{345})\lambda_6 + (2\lambda_2 + \lambda_{345})\lambda_7 \Big], \quad (B.8)
$$

$$
\mathcal{D}v_2 = \frac{v_2}{16\pi^2}\left[\frac{3}{4}(3g_2^2 + g'^2) - 3y_t^2 \right]
$$

$$
+ \frac{v_2}{256\pi^4}\Bigg[\frac{435}{32}g_2^4 - \frac{149}{32}g'^4 - \frac{3}{16}g_2^2 g'^2 - 6\lambda_2^2 - \lambda_3^2 - \lambda_3\lambda_4 - \lambda_4^2
$$

$$
- \frac{3}{2}(\lambda_5^2 + \lambda_6^2 + 3\lambda_7^2) + \left(20g_3^2 + \frac{45}{8}g_2^2 + \frac{85}{24}g'^2 \right) y_t^2 + \frac{9}{4}y_b^2 y_t^2 + \frac{27}{4}y_t^4 \Bigg]
$$

$$
- \frac{3v_1}{512\pi^4}\Big[(2\lambda_1 + \lambda_{345})\lambda_6 + (2\lambda_2 + \lambda_{345})\lambda_7 \Big] . \quad (B.9)
$$

The two-loop RGEs for all the scalar quartic couplings appearing in (1.2) in the Type-II

2HDM are given by

$$
\begin{aligned}
\mathcal{D}\lambda_1 \;=\; &\frac{1}{16\pi^2}\Bigg[\frac{3}{8}(3g_2^4 + g'^4 + 2g_2^2g'^2) - 3\lambda_1(3g_2^2 + g'^2) + 24\lambda_1^2 + 2\lambda_3^2 + 2\lambda_3\lambda_4 + \lambda_4^2 \\
&\qquad + \lambda_5^2 + 12\lambda_6^2 + 4\lambda_1(3y_b^2 + y_\tau^2) - 6y_b^4 - 2y_\tau^4\Bigg] \\
&+ \frac{1}{256\pi^4}\Bigg[\frac{1}{16}\left(291g_2^6 - 101g_2^4g'^2 - 191g_2^2g'^4 - 131g'^6\right) \\
&- \frac{1}{8}(51g_2^4 - 78g_2^2g'^2 - 217g'^4)\lambda_1 + \frac{5}{2}(3g_2^4 + g'^4)\lambda_3 + \frac{5}{4}(3g_2^4 + 2g_2^2g'^2 + g'^4)\lambda_4 \\
&+ (3g_2^2 + g'^2)(36\lambda_1^2 + 4\lambda_3^2 + 4\lambda_3\lambda_4 + \lambda_4^2 + 18\lambda_6^2) + g'^2(\lambda_4^2 - \lambda_5^2) - 312\lambda_1^3 \\
&- 20\lambda_1\lambda_3^2 - 8\lambda_3^3 - 6\lambda_4^3 - 20\lambda_1\lambda_3\lambda_4 - 4(5\lambda_1 + 3\lambda_4)\lambda_3^2 - 4(3\lambda_1 + 4\lambda_3)\lambda_4^2 \\
&- 2(7\lambda_1 + 10\lambda_3 + 11\lambda_4)\lambda_5^2 - 2(159\lambda_1 + 33\lambda_3 + 35\lambda_4 + 37\lambda_5)\lambda_6^2 \\
&- 4(9\lambda_3 + 7\lambda_4 + 5\lambda_5)\lambda_6\lambda_7 + 2(3\lambda_1 - 9\lambda_3 - 7\lambda_4 - 5\lambda_5)\lambda_7^2 \\
&- \left\{\frac{9}{4}g_2^4 - \frac{9}{2}g_2^2g'^2 - \frac{5}{4}g'^4 - \left(\frac{45}{2}g_2^2 + 80g_3^2 + \frac{25}{6}g'^2\right)\lambda_1 + 36(4\lambda_1^2 + \lambda_6^2)\right\}y_b^2 \\
&- \left(32g_3^2 - \frac{4}{3}g'^2 + 3\lambda_1\right)y_b^4 - 6(2\lambda_3^2 + 2\lambda_3\lambda_4 + \lambda_4^2 + \lambda_5^2 + 6\lambda_6^2)y_t^2 \\
&- \left\{\frac{3}{4}g_2^4 - \frac{11}{2}g_2^2g'^2 + \frac{25}{4}g'^4 - \frac{5}{2}(3g_2^2 + 5g'^2)\lambda_1 + 12(4\lambda_1^2 + \lambda_6^2)\right\}y_\tau^2 \\
&- (4g'^2 + \lambda_1)y_\tau^4 - 9\lambda_1 y_b^2 y_t^2 - 6y_t^2 y_b^4 + 30y_b^6 + 10y_\tau^6\Bigg]\,, \qquad\qquad\text{(B.10)}
\end{aligned}
$$

$$
\begin{aligned}
\mathcal{D}\lambda_2 \;=\; &\frac{1}{16\pi^2}\Bigg[\frac{3}{8}(3g_2^4 + g'^4 + 2g_2^2g'^2) - 3\lambda_2(3g_2^2 + g'^2) + 24\lambda_2^2 + 2\lambda_3^2 + 2\lambda_3\lambda_4 \\
&\qquad + \lambda_4^2 + \lambda_5^2 + 12\lambda_7^2 + 12\lambda_2 y_t^2 - 6y_t^4\Bigg] \\
&+ \frac{1}{256\pi^4}\Bigg[\frac{1}{16}\left(291g_2^6 - 101g_2^4g'^2 - 191g_2^2g'^4 - 131g'^6\right) \\
&- \frac{1}{8}\left(51g_2^4 - 78g_2^2g'^2 - 217g'^4\right)\lambda_2 + \frac{5}{2}(3g_2^4 + g'^4)\lambda_3 + \frac{5}{4}(3g_2^4 + 2g_2^2g'^2 + g'^4)\lambda_4 \\
&+ (3g_2^2 + g'^2)(36\lambda_2^2 + 4\lambda_3^2 + 4\lambda_3\lambda_4 + \lambda_4^2 + 18\lambda_7^2) + g'^2(\lambda_4^2 - \lambda_5^2) - 312\lambda_2^3 \\
&- 20\lambda_2\lambda_3^2 - 8\lambda_3^3 - 6\lambda_4^3 - 20\lambda_2\lambda_3\lambda_4 - 4(5\lambda_2 + 3\lambda_3)\lambda_3^2 - 4(3\lambda_2 + 4\lambda_3)\lambda_4^2 \\
&- 2(7\lambda_2 + 10\lambda_3 + 11\lambda_4)\lambda_5^2 + 2(3\lambda_2 - 9\lambda_3 - 7\lambda_4 - 5\lambda_5)\lambda_6^2 \\
&- 4(9\lambda_3 + 7\lambda_4 + 5\lambda_5)\lambda_6\lambda_7 - 2(159\lambda_2 + 33\lambda_3 + 35\lambda_4 + 37\lambda_5)\lambda_7^2 \\
&- 6(2\lambda_3^2 + 2\lambda_3\lambda_4 + \lambda_4^2 + \lambda_5^2 + 6\lambda_7^2)y_b^2 - \left\{\frac{9}{4}g_2^4 - \frac{21}{2}g_2^2g'^2 + \frac{19}{4}g'^4\right. \\
&- \left.\left(\frac{45}{2}g_2^2 + 80g_3^2 + \frac{85}{6}g'^2\right)\lambda_2 + 36(4\lambda_2^2 + \lambda_7^2)\right\}y_t^2 - 9\lambda_2 y_b^2 y_t^2 - 6y_b^2 y_t^4 \\
&- \left(32g_3^2 + \frac{8}{3}g'^2 + 3\lambda_2\right)y_t^4 + 30y_t^6 - 2(2\lambda_3^2 + 2\lambda_3\lambda_4 + \lambda_4^2 + \lambda_5^2 + 6\lambda_7^2)y_\tau^2\Bigg]\,, \text{ (B.11)}
\end{aligned}
$$

$$\mathcal{D}\lambda_3 = \frac{1}{16\pi^2}\left[\frac{3}{4}(3g_2^4 + g'^4 - 2g_2^2 g'^2) - 3\lambda_3(3g_2^2 + g'^2) + 4(\lambda_1 + \lambda_2)(3\lambda_3 + \lambda_4) + 4\lambda_3^2\right.$$

$$\left. + 2(\lambda_4^2 + \lambda_5^2) + 4(\lambda_6^2 + \lambda_7^2 + 4\lambda_6\lambda_7) + 2\lambda_3(3y_b^2 + y_\tau^2 + 3y_t^2) - 12y_b^2 y_t^2\right]$$

$$+ \frac{1}{256\pi^4}\left[\frac{1}{8}\left(291g_2^6 + 11g_2^4 g'^2 + 101g_2^2 g'^4 - 131g'^6\right)\right.$$

$$+ \frac{5}{2}\left(9g_2^4 - 2g_2^2 g'^2 + 3g'^4\right)(\lambda_1 + \lambda_2) - \frac{1}{8}(111g_2^4 - 22g_2^2 g'^2 - 197g'^4)\lambda_3$$

$$+ 2(3g_2^2 + g'^2)[12(\lambda_1 + \lambda_2)\lambda_3 + \lambda_3^2 + \lambda_4^2] - 4(\lambda_1^2 + \lambda_2^2)(15\lambda_3 + 4\lambda_4)$$

$$- 4(\lambda_1 + \lambda_2)(18\lambda_3^2 + 7\lambda_4^2 + 8\lambda_3\lambda_4 + 9\lambda_5^2) - 12(\lambda_3^3 + \lambda_4^3 + g_2^2\lambda_3\lambda_4)$$

$$+ \left(\frac{15}{2}g_2^4 - 3g_2^2 g'^2 + \frac{5}{2}g'^4\right)\lambda_4 + 4(9g_2^2 + 2g'^2)(\lambda_1 + \lambda_2)\lambda_4$$

$$- 4\lambda_3\lambda_4(\lambda_3 + 4\lambda_4) - 2(9\lambda_3 + 22\lambda_4)\lambda_5^2 - 4g'^2(\lambda_4^2 - \lambda_5^2) + 2g'^2(\lambda_6^2 + \lambda_7^2)$$

$$- 4(31\lambda_1 + 11\lambda_2)\lambda_6^2 - 4(15\lambda_3 + 17\lambda_4 + 17\lambda_5)(\lambda_6^2 + \lambda_7^2) + 4(27g_2^2 + 8g'^2)\lambda_6\lambda_7$$

$$- 8[11(\lambda_1 + \lambda_2 + 2\lambda_3 + \lambda_4) + 9\lambda_5]\lambda_6\lambda_7 - 4(11\lambda_1 + 31\lambda_2)\lambda_7^2$$

$$- \left\{\frac{1}{4}(9g_2^4 - 5g'^4 + 18g_2^2 g'^2) - \left(40g_3^2 + \frac{45}{4}g_2^2 + \frac{25}{12}g'^2\right)\lambda_3\right\}y_b^2$$

$$- \frac{1}{4}\left\{3g_2^4 + 25g'^4 + 22g_2^2 g'^2 + 5(3g_2^2 + 5g'^2)\lambda_3\right\}y_\tau^2$$

$$- \left\{(2\lambda_3^2 + \lambda_4^2 + 4\lambda_1(3\lambda_3 + \lambda_4) + \lambda_5^2 + 4\lambda_6^2 + 8\lambda_6\lambda_7)\right\}(3y_b^2 + y_\tau^2)$$

$$- \left\{\frac{9}{4}g_2^4 + \frac{21}{2}g_2^2 g'^2 + \frac{19}{4}g'^4 - \left(40g_3^2 + \frac{45}{4}g_2^2 + \frac{85}{12}g'^2\right)\lambda_3\right.$$

$$\left. + 6(12\lambda_2\lambda_3 + 2\lambda_3^2 + 4\lambda_2\lambda_4 + \lambda_4^2 + \lambda_5^2 + 8\lambda_6\lambda_7 + 4\lambda_7^2)\right\}y_t^2$$

$$\left. - \left(64g_3^2 + \frac{4}{3}g'^2 - 15\lambda_3\right)y_b^2 y_t^2 + 36y_b^4 y_t^2 - \frac{9}{2}\lambda_3[3(y_b^4 + y_t^4) + y_\tau^4] + 36y_b^2 y_t^4\right], \quad \text{(B.12)}$$

$$\mathcal{D}\lambda_4 = \frac{1}{16\pi^2}\left[3g_2^2 g'^2 - 3\lambda_4(3g_2^2 + g'^2) + 4(\lambda_1 + \lambda_2 + 2\lambda_3)\lambda_4 + 4\lambda_4^2 + 8\lambda_5^2\right.$$

$$\left. + 10(\lambda_6^2 + \lambda_7^2) + 4\lambda_6\lambda_7 + 2\lambda_4\{3(y_b^2 + y_t^2) + y_\tau^2\} + 12y_b^2 y_t^2\right]$$

$$+ \frac{1}{256\pi^4}\left[-14g_2^4 g'^2 - \frac{73}{2}g_2^2 g'^4 + 2g_2^2 g'^2\{5(\lambda_1 + \lambda_2) + \lambda_3\}\right.$$

$$- \frac{1}{8}(231g_2^4 - 102g_2^2 g'^2 - 157g'^4)\lambda_4 + 4\{2g'^2(\lambda_1 + \lambda_2) - 7(\lambda_1^2 + \lambda_2^2 + \lambda_3^2)\}\lambda_4$$

$$+ 4(9g_2^2 + g'^2)\lambda_3\lambda_4 - 40(\lambda_1 + \lambda_2)(2\lambda_3\lambda_4 + \lambda_4^2) + 2(9g_2^2 + 4g'^2)\lambda_4^2 - 28\lambda_3\lambda_4^2$$

$$+ 2(27g_2^2 + 8g'^2)\lambda_5^2 - 48(\lambda_1 + \lambda_2 + \lambda_3)\lambda_5^2 - 26\lambda_4\lambda_5^2 + 8g'^2\lambda_6\lambda_7$$

$$+ 2\{27g_2^2 + 7g'^2 - 2(18\lambda_3 + 17\lambda_4 + 20\lambda_5)\}(\lambda_6^2 + \lambda_7^2) - 4(37\lambda_1 + 5\lambda_2)\lambda_6^2$$

$$- 8\{5(\lambda_1 + \lambda_2 + 2\lambda_3 + 4\lambda_4) + 12\lambda_5\}\lambda_6\lambda_7 - 4(5\lambda_1 + 37\lambda_2)\lambda_7^2$$

$$+ \left\{9g_2^2 g'^2 + \left(40g_3^2 + \frac{45}{4}g_2^2 + \frac{25}{12}g'^2\right)\lambda_4 - 12[2(\lambda_1 + \lambda_3)\lambda_4 + \lambda_4^2 + 2\lambda_5^2\right.$$

$$+ 5\lambda_6^2 + \lambda_6\lambda_7\Big\}y_b^2 + \Big\{21g_2^2 g'^2 + \Big(40g_3^2 + \frac{45}{4}g_2^2 + \frac{85}{12}g'^2\Big)\lambda_4 - 12[2(\lambda_2 + \lambda_3)\lambda_4$$

$$+ \lambda_4^2 + 2\lambda_5^2 + \lambda_6\lambda_7 + 5\lambda_7^2]\Big\}y_t^2 + \Big(64g_3^2 + \frac{4}{3}g'^2 - 24\lambda_3 - 33\lambda_4\Big)y_b^2 y_t^2$$

$$+ \Big\{11g_2^2 g'^2 + \frac{5}{4}\left(3g_2^2 + 5g'^2\right)\lambda_4 - 8(\lambda_1 + \lambda_3)\lambda_4 - 4\lambda_4^2 - 8\lambda_5^2$$

$$- 20\lambda_6^2 - 4\lambda_6\lambda_7\Big\}y_\tau^2 - \frac{9}{2}\lambda_4\{3(y_b^4 + y_t^4) + y_\tau^4 - 24y_b^2 y_t^2(y_b^2 + y_t^2)\}\Bigg], \qquad \text{(B.13)}$$

$$\mathcal{D}\lambda_5 = \frac{1}{16\pi^2}\Bigg[-3\lambda_5(3g_2^2 + g'^2) + 4(\lambda_1 + \lambda_2 + 2\lambda_3 + 3\lambda_4)\lambda_5 + 10(\lambda_6^2 + \lambda_7^2)$$

$$+ 4\lambda_6\lambda_7 + 2\lambda_5\{3(y_b^2 + y_t^2) + y_\tau^2\}\Bigg]$$

$$+ \frac{1}{256\pi^4}\Bigg[-\frac{1}{8}\Big(231g_2^4 - 38g_2^2 g'^2 - 157g'^4\Big)\lambda_5 + 4(9g_2^2 + 4g'^2)\lambda_3\lambda_5$$

$$- 4\Big\{g'^2(\lambda_1 + \lambda_2) + 7(\lambda_1^2 + \lambda_2^2 + \lambda_3^2)\Big\}\lambda_5 - 8(\lambda_1 + \lambda_2)(10\lambda_3 + 11\lambda_4)\lambda_5$$

$$+ 4\{6(3g_2^2 + g'^2) - 19\lambda_3 - 8\lambda_4\}\lambda_4\lambda_5 + 6\lambda_5^3 - 4(37\lambda_1 + 5\lambda_2)\lambda_6^2$$

$$- 4(5\lambda_1 + 37\lambda_2)\lambda_7^2 + 2\{27g_2^2 + 10g'^2 - 2(18\lambda_3 + 19\lambda_4 + 18\lambda_5)\}(\lambda_6^2 + \lambda_7^2)$$

$$- 4\{g'^2 + 10(\lambda_1 + \lambda_2 + 2\lambda_3) + 22\lambda_4 + 37\lambda_5\}\lambda_6\lambda_7$$

$$+ \Big\{\Big(40g_3^2 + \frac{45}{4}g_2^2 + \frac{25}{12}g'^2\Big)\lambda_5 - 12[2(\lambda_1 + \lambda_3)\lambda_5 + 3\lambda_4\lambda_5 + 5\lambda_6^2 + \lambda_6\lambda_7]\Big\}y_b^2$$

$$+ \Big\{\Big(40g_3^2 + \frac{45}{2}g_2^2 + \frac{85}{12}g'^2\Big)\lambda_5 - 12[2(\lambda_2 + \lambda_3)\lambda_5 + 3\lambda_4\lambda_5 + \lambda_6\lambda_7 + 5\lambda_7^2]\Big\}y_t^2$$

$$+ \Big\{\Big(\frac{15}{4}g_2^2 + \frac{25}{4}g'^2\Big)\lambda_5 - 8(\lambda_1 + \lambda_3)\lambda_5 - 12\lambda_4\lambda_5 - 20\lambda_6^2 - 4\lambda_6\lambda_7\Big\}y_\tau^2$$

$$- \frac{1}{2}\lambda_5\{3(y_b^4 + y_t^4) + y_\tau^4\} - 33\lambda_5 y_b^2 y_t^2\Bigg], \qquad \text{(B.14)}$$

$$\mathcal{D}\lambda_6 = \frac{1}{16\pi^2}\Bigg[-3\lambda_6(3g_2^2 + g'^2) + 2(12\lambda_1 + 3\lambda_3 + 4\lambda_4)\lambda_6 + 2(3\lambda_3 + 2\lambda_4)\lambda_7$$

$$+ 10\lambda_5\lambda_6 + 2\lambda_5\lambda_7 + 3\lambda_6(3y_b^2 + y_t^2 + y_\tau^2)\Bigg]$$

$$+ \frac{1}{256\pi^4}\Bigg[-\frac{1}{8}(141g_2^4 - 58g_2^2 g'^2 - 187g'^4)\lambda_6 + 6(3g_2^2 + g'^2)(6\lambda_1 + \lambda_3)\lambda_6$$

$$- 6(53\lambda_1^2 + \lambda_2^2)\lambda_6 - 4(33\lambda_1 + 9\lambda_2 + 8\lambda_3)\lambda_3\lambda_6 + 2(18g_2^2 + 5g'^2)\lambda_4\lambda_6$$

$$- 2(70\lambda_1 + 14\lambda_2 + 34\lambda_3 + 17\lambda_4)\lambda_4\lambda_6 + 2(27g_2^2 + 10g'^2)\lambda_5\lambda_6$$

$$- 4(37\lambda_1 + 5\lambda_2 + 18\lambda_3 + 19\lambda_4 + 9\lambda_5)\lambda_5\lambda_6 - 111\lambda_6^3 - 42\lambda_7^3$$

$$+ \frac{5}{4}(9g_2^4 + 2g_2^2 g'^2 + 3g'^4)\lambda_7 + 12(3g_2^2 + g'^2)\lambda_3\lambda_7 - 36(\lambda_1 + \lambda_2 + \lambda_3)\lambda_3\lambda_7$$

$$+ 2(9g_2^2\lambda_4 + 4g'^2)\lambda_4\lambda_7 - 2\{14(\lambda_1 + \lambda_2 + 2\lambda_3)\lambda_4 + 17\lambda_4\}\lambda_4\lambda_7$$

$$- 2\{g'^2 + 10(\lambda_1 + \lambda_2 + 2\lambda_3) + 22\lambda_4 + 21\lambda_5\}\lambda_5\lambda_7 - 3(42\lambda_6 + 11\lambda_7)\lambda_6\lambda_7$$

$$
+ \left\{ 60g_3^2 + \frac{135}{8}g_2^2 + \frac{25}{8}g'^2 - 6(24\lambda_1 + 3\lambda_3 + 4\lambda_4 + 5\lambda_5) \right\} \lambda_6 y_b^2
$$

$$
+ \left\{ 20g_3^2 + \frac{45}{8}g_2^2 + \frac{85}{24}g'^2 - 6(3\lambda_3 + 4\lambda_4 + 5\lambda_5) \right\} \lambda_6 y_t^2
$$

$$
+ \left\{ \frac{15}{8}(3g_2^2 + 5g'^2) - 2(\lambda_1 + 3\lambda_3 + 4\lambda_4 + 5\lambda_5) \right\} \lambda_6 y_\tau^2
$$

$$
- 12(3\lambda_3 + 2\lambda_4 + \lambda_5)\lambda_7 y_t^2 - \frac{1}{4}(27y_t^4 + 33y_b^4 + 11y_\tau^4)\lambda_6 - 21\lambda_6 y_b^2 y_t^2 \bigg] , \qquad \text{(B.15)}
$$

$$
\mathcal{D}\lambda_7 = \frac{1}{16\pi^2} \bigg[-3\lambda_7(3g_2^2 + g'^2) + 2(12\lambda_2 + 3\lambda_3 + 4\lambda_4)\lambda_7 + 2(3\lambda_3 + 2\lambda_4)\lambda_6
$$

$$
+ 10\lambda_5\lambda_7 + 2\lambda_5\lambda_6 + \lambda_7(3y_b^2 + 9y_t^2 + y_\tau^2) \bigg]
$$

$$
+ \frac{1}{256\pi^4} \bigg[\frac{5}{4}(9g_2^4 + 2g_2^2 g'^2 + 3g'^4)\lambda_6 + 12(3g_2^2 + g'^2)\lambda_3\lambda_6
$$

$$
- 36(\lambda_1 + \lambda_2 + \lambda_3)\lambda_3 + 2(9g_2^2 + 4g'^2)\lambda_4\lambda_6 - 28(\lambda_1 + \lambda_2 + 2\lambda_3)\lambda_4\lambda_6
$$

$$
- 34\lambda_4^2\lambda_6 - 2g'^2\lambda_5\lambda_6 - 4\{5(\lambda_1 + \lambda_2 + 2\lambda_3) + 11\lambda_4\}\lambda_5\lambda_6 - 42(\lambda_5^2 + \lambda_6^2)\lambda_6
$$

$$
- \frac{1}{8}(141g_2^4 - 58g_2^2 g'^2 - 187g'^4)\lambda_7 + 6\lambda_1^2\lambda_7 + 36(3g_2^2 + g'^2)\lambda_2\lambda_7 - 318\lambda_2^2\lambda_7
$$

$$
+ 6(3g_2^2 + g'^2)\lambda_3\lambda_7 - 12(3\lambda_1 + 11\lambda_2)\lambda_3\lambda_7 - 32\lambda_3^2\lambda_7 + 2(18g_2^2 + 5g'^2)\lambda_4\lambda_7
$$

$$
- 4(7\lambda_1 + 35\lambda_2 + 17\lambda_3)\lambda_4\lambda_7 - 34\lambda_4^2\lambda_7 + 2(27g_2^2 + 10g'^2)\lambda_5\lambda_7
$$

$$
- 4(5\lambda_1 + 37\lambda_2 + 18\lambda_3 + 19\lambda_4)\lambda_5\lambda_7 - 36\lambda_5^2\lambda_7 - 33\lambda_6^2\lambda_7
$$

$$
- 126\lambda_6\lambda_7^2 - 111\lambda_7^3 - 12(3\lambda_3 + 2\lambda_4 + \lambda_5)\lambda_6 y_b^2
$$

$$
+ \left\{ 20g_3^2 + \frac{45}{8}g_2^2 + \frac{25}{24}g'^2 - 6(3\lambda_3 + 4\lambda_4 + 5\lambda_5) \right\} \lambda_7 y_b^2
$$

$$
+ \left\{ 60g_3^2 + \frac{135}{8}g_2^2 + \frac{85}{8}g'^2 - 6(24\lambda_2 + 3\lambda_3 + 4\lambda_4 + 5\lambda_5) \right\} \lambda_7 y_t^2
$$

$$
- 4(3\lambda_3 + 2\lambda_4 + \lambda_5)\lambda_6 y_\tau^2 + \left\{ \frac{5}{8}(3g_2^2 + 5g'^2) - 6\lambda_3 - 8\lambda_4 - 10\lambda_5 \right\} \lambda_7 y_\tau^2
$$

$$
- \frac{1}{4}(33y_t^4 + 27y_b^4 + 9y_\tau^4)\lambda_7 - 21\lambda_7 y_b^2 y_t^2 \bigg] . \qquad \text{(B.16)}
$$

Finally, the two-loop RGE for the soft mass parameter is given by

$$
\mathcal{D}(m_{12}^2) = \frac{1}{16\pi^2} \bigg[-\frac{3}{2}(3g_2^2 + g'^2)m_{12}^2 + 2(\lambda_3 + 2\lambda_4 + 3\lambda_5)m_{12}^2
$$

$$
+ 2(3y_b^2 + 3y_t^2 + y_\tau^2)m_{12}^2 + 12(\lambda_6\mu_1^2 + \lambda_7\mu_2^2) \bigg]
$$

$$
+ \frac{1}{256\pi^4} \bigg[-\frac{1}{16}(243g_2^4 - 30g_2^2 g'^2 - 153g'^4)m_{12}^2 + 3\{2\lambda_1^2 + \lambda_2^2) + \lambda_5^2
$$

$$
+ 4(\lambda_6^2 + \lambda_7^2)\}m_{12}^2 + 4(3g_2^2 + g'^2)(\lambda_3 + 2\lambda_4 + 3\lambda_5)m_{12}^2
$$

$$
\begin{aligned}
&- 12(\lambda_1 + \lambda_2)\lambda_{345}m_{12}^2 - 6(\lambda_3\lambda_4 + 2\lambda_3\lambda_5 + 2\lambda_4\lambda_5 + 6\lambda_6\lambda_7)m_{12}^2 \\
&+ \left\{20g_3^2 + \frac{45}{8}g_2^2 + \frac{25}{24}g'^2 - 6(\lambda_3 + 2\lambda_4 + 3\lambda_5)\right\}y_b^2 m_{12}^2 \\
&+ \left\{20g_3^2 + \frac{45}{8}g_2^2 + \frac{85}{24}g'^2 - 6(\lambda_3 + 2\lambda_4 + 3\lambda_5)\right\}y_t^2 m_{12}^2 \\
&+ \left\{\frac{5}{8}(3g_2^2 + 5g'^2) - 2(\lambda_3 + 2\lambda_4 + 3\lambda_5)\right\}y_\tau^2 m_{12}^2 \\
&+ 24(3g_2^2 + g'^2)(\lambda_6\mu_1^2 + \lambda_7\mu_2^2) - 72(\lambda_1\lambda_6\mu_1^2 + \lambda_2\lambda_7\mu_2^2) \\
&- 12\lambda_{345}\{(2\lambda_6 + \lambda_7)\mu_1^2 + (\lambda_6 + 2\lambda_7)\mu_2^2\} \\
&- 24\{(3y_b^2 + y_\tau^2)\lambda_6\mu_1^2 + 3y_t^2\lambda_7\mu_2^2\} - \frac{9}{4}(3y_b^4 + 3y_t^4 + y_\tau^4)m_{12}^2 \Bigg] \quad\quad (\text{B.17})
\end{aligned}
$$

Note that the mass parameters $\mu_{1,2}^2$ are removed by the tadpole conditions:

$$
\frac{\partial V}{\partial v_1} = 0 = -\mu_1^2 v_1 - m_{12}^2 v_2 + \frac{1}{2}\left[2\lambda_1 v_1^3 + \lambda_{345}v_1 v_2^2 + 3\lambda_6 v_1^2 v_2 + \lambda_7 v_2^3\right], \quad (\text{B.18})
$$

$$
\frac{\partial V}{\partial v_2} = 0 = -\mu_2^2 v_2 - m_{12}^2 v_1 + \frac{1}{2}\left[2\lambda_2 v_2^3 + \lambda_{345}v_2 v_1^2 + \lambda_6 v_1^3 + 3\lambda_7 v_2 v_1^2\right], \quad (\text{B.19})
$$

and hence, it is not necessary to write down their RGEs explicitly.

References

[1] ATLAS collaboration, *Observation of a new particle in the search for the Standard Model Higgs boson with the ATLAS detector at the LHC*, *Phys. Lett.* **B 716** (2012) 1 [arXiv:1207.7214] [INSPIRE].

[2] CMS collaboration, *Observation of a new boson at a mass of 125 GeV with the CMS experiment at the LHC*, *Phys. Lett.* **B 716** (2012) 30 [arXiv:1207.7235] [INSPIRE].

[3] ATLAS collaboration, *Updated coupling measurements of the Higgs boson with the ATLAS detector using up to 25 fb^{-1} of proton-proton collision data*, ATLAS-CONF-2014-009 (2014).

[4] CMS collaboration, *Precise determination of the mass of the Higgs boson and studies of the compatibility of its couplings with the standard model*, CMS-PAS-HIG-14-009 (2014).

[5] J.F. Gunion, H.E. Haber, G. Kane and S. Dawson, *The Higgs Hunter's Guide*, Addison-Wesley (1990).

[6] G.C. Branco et al., *Theory and phenomenology of two-Higgs-doublet models*, *Phys. Rept.* **516** (2012) 1 [arXiv:1106.0034] [INSPIRE].

[7] R.A. Battye, G.D. Brawn and A. Pilaftsis, *Vacuum Topology of the Two Higgs Doublet Model*, *JHEP* **08** (2011) 020 [arXiv:1106.3482] [INSPIRE].

[8] S.L. Glashow and S. Weinberg, *Natural Conservation Laws for Neutral Currents*, *Phys. Rev.* **D 15** (1977) 1958 [INSPIRE].

[9] E.A. Paschos, *Diagonal Neutral Currents*, *Phys. Rev.* **D 15** (1977) 1966 [INSPIRE].

[10] A. Pich and P. Tuzon, *Yukawa Alignment in the Two-Higgs-Doublet Model*, *Phys. Rev.* **D 80** (2009) 091702 [arXiv:0908.1554] [INSPIRE].

[11] ATLAS collaboration, *Constraints on New Phenomena via Higgs Coupling Measurements with the ATLAS Detector*, ATLAS-CONF-2014-010 (2014).

[12] A. Celis, V. Ilisie and A. Pich, *LHC constraints on two-Higgs doublet models*, *JHEP* **07** (2013) 053 [arXiv:1302.4022] [INSPIRE].

[13] C.-Y. Chen, S. Dawson and M. Sher, *Heavy Higgs Searches and Constraints on Two Higgs Doublet Models*, *Phys. Rev.* **D 88** (2013) 015018 [arXiv:1305.1624] [INSPIRE].

[14] N. Craig, J. Galloway and S. Thomas, *Searching for Signs of the Second Higgs Doublet*, arXiv:1305.2424 [INSPIRE].

[15] K. Cheung, J.S. Lee and P.-Y. Tseng, *Higgcision in the Two-Higgs Doublet Models*, *JHEP* **01** (2014) 085 [arXiv:1310.3937] [INSPIRE].

[16] L. Wang and X.-F. Han, *Study of the heavy CP-even Higgs with mass 125 GeV in two-Higgs-doublet models at the LHC and ILC*, arXiv:1404.7437 [INSPIRE].

[17] B. Dumont, J.F. Gunion, Y. Jiang and S. Kraml, *Constraints on and future prospects for Two-Higgs-Doublet Models in light of the LHC Higgs signal*, *Phys. Rev.* **D 90** (2014) 035021 [arXiv:1405.3584] [INSPIRE].

[18] S. Kanemura, K. Tsumura, K. Yagyu and H. Yokoya, *Fingerprinting non-minimal Higgs sectors*, arXiv:1406.3294 [INSPIRE].

[19] C.-W. Chiang and K. Yagyu, *Implications of Higgs boson search data on the two-Higgs doublet models with a softly broken Z_2 symmetry*, *JHEP* **07** (2013) 160 [arXiv:1303.0168] [INSPIRE].

[20] B. Grinstein and P. Uttayarat, *Carving Out Parameter Space in Type-II Two Higgs Doublets Model*, *JHEP* **06** (2013) 094 [*Erratum ibid.* **1309** (2013) 110] [arXiv:1304.0028] [INSPIRE].

[21] O. Eberhardt, U. Nierste and M. Wiebusch, *Status of the two-Higgs-doublet model of type-II*, *JHEP* **07** (2013) 118 [arXiv:1305.1649] [INSPIRE].

[22] J. Baglio, O. Eberhardt, U. Nierste and M. Wiebusch, *Benchmarks for Higgs Pair Production and Heavy Higgs Searches in the Two-Higgs-Doublet Model of Type II*, *Phys. Rev.* **D 90** (2014) 015008 [arXiv:1403.1264] [INSPIRE].

[23] P.H. Chankowski et al., *Do precision electroweak constraints guarantee e^+e^- collider discovery of at least one Higgs boson of a two Higgs doublet model?*, *Phys. Lett.* **B 496** (2000) 195 [hep-ph/0009271] [INSPIRE].

[24] J.F. Gunion and H.E. Haber, *The CP conserving two Higgs doublet model: The Approach to the decoupling limit*, *Phys. Rev.* **D 67** (2003) 075019 [hep-ph/0207010] [INSPIRE].

[25] I.F. Ginzburg and M. Krawczyk, *Symmetries of two Higgs doublet model and CP-violation*, *Phys. Rev.* **D 72** (2005) 115013 [hep-ph/0408011] [INSPIRE].

[26] M. Carena, I. Low, N.R. Shah and C.E.M. Wagner, *Impersonating the Standard Model Higgs Boson: Alignment without Decoupling*, *JHEP* **04** (2014) 015 [arXiv:1310.2248] [INSPIRE].

[27] A. Delgado, G. Nardini and M. Quirós, *A Light Supersymmetric Higgs Sector Hidden by a Standard Model-like Higgs*, *JHEP* **07** (2013) 054 [arXiv:1303.0800] [INSPIRE].

[28] C.C. Nishi, *Custodial* SO(4) *symmetry and CP-violation in N-Higgs-doublet potentials*, *Phys. Rev.* **D 83** (2011) 095005 [arXiv:1103.0252] [INSPIRE].

[29] A. Pilaftsis, *On the Classification of Accidental Symmetries of the Two Higgs Doublet Model Potential*, *Phys. Lett.* **B 706** (2012) 465 [arXiv:1109.3787] [INSPIRE].

[30] M. Maniatis, A. von Manteuffel and O. Nachtmann, *CP violation in the general two-Higgs-doublet model: A Geometric view*, *Eur. Phys. J.* **C 57** (2008) 719 [arXiv:0707.3344] [INSPIRE].

[31] I.P. Ivanov, *Minkowski space structure of the Higgs potential in 2HDM. II. Minima, symmetries and topology*, *Phys. Rev.* **D 77** (2008) 015017 [arXiv:0710.3490] [INSPIRE].

[32] C.C. Nishi, *Physical parameters and basis transformations in the Two-Higgs-Doublet model*, *Phys. Rev.* **D 77** (2008) 055009 [arXiv:0712.4260] [INSPIRE].

[33] N.G. Deshpande and E. Ma, *Pattern of Symmetry Breaking with Two Higgs Doublets*, *Phys. Rev.* **D 18** (1978) 2574 [INSPIRE].

[34] J. Patera, R.T. Sharp and R. Slansky, *On a new relation between semisimple Lie algebras*, *J. Math. Phys.* **21** (1980) 2335 [INSPIRE].

[35] R. Slansky, *Group Theory for Unified Model Building*, *Phys. Rept.* **79** (1981) 1 [INSPIRE].

[36] P. Sikivie, L. Susskind, M.B. Voloshin and V.I. Zakharov, *Isospin Breaking in Technicolor Models*, *Nucl. Phys.* **B 173** (1980) 189 [INSPIRE].

[37] J.F. Gunion and H.E. Haber, *Conditions for CP-violation in the general two-Higgs-doublet model*, *Phys. Rev.* **D 72** (2005) 095002 [hep-ph/0506227] [INSPIRE].

[38] M. Maniatis and O. Nachtmann, *Symmetries and renormalisation in two-Higgs-doublet models*, *JHEP* **11** (2011) 151 [arXiv:1106.1436] [INSPIRE].

[39] J. Goldstone, *Field Theories with Superconductor Solutions*, *Nuovo Cim.* **19** (1961) 154 [INSPIRE].

[40] PARTICLE DATA GROUP collaboration, K.A. Olive et al., *The Review of Particle Physics*, *Chin. Phys.* **C 38** (2014) 090001 [http://pdg.lbl.gov/].

[41] R.D. Peccei and H.R. Quinn, *CP Conservation in the Presence of Instantons*, *Phys. Rev. Lett.* **38** (1977) 1440 [INSPIRE].

[42] H.E. Haber and R. Hempfling, *The Renormalization group improved Higgs sector of the minimal supersymmetric model*, *Phys. Rev.* **D 48** (1993) 4280 [hep-ph/9307201] [INSPIRE].

[43] A. Pilaftsis and C.E.M. Wagner, *Higgs bosons in the minimal supersymmetric standard model with explicit CP-violation*, *Nucl. Phys.* **B 553** (1999) 3 [hep-ph/9902371] [INSPIRE].

[44] H. Georgi and D.V. Nanopoulos, *Suppression of Flavor Changing Effects From Neutral Spinless Meson Exchange in Gauge Theories*, *Phys. Lett.* **B 82** (1979) 95 [INSPIRE].

[45] J.F. Donoghue and L.F. Li, *Properties of Charged Higgs Bosons*, *Phys. Rev.* **D 19** (1979) 945 [INSPIRE].

[46] L. Lavoura and J.P. Silva, *Fundamental CP-violating quantities in a SU(2)×U(1) model with many Higgs doublets*, *Phys. Rev.* **D 50** (1994) 4619 [hep-ph/9404276] [INSPIRE].

[47] F.J. Botella and J.P. Silva, *Jarlskog - like invariants for theories with scalars and fermions*, *Phys. Rev.* **D 51** (1995) 3870 [hep-ph/9411288] [INSPIRE].

[48] M. Carena, H.E. Haber, I. Low, N.R. Shah and C.E.M. Wagner, *Complementarity Between Non-Standard Higgs Searches and Precision Higgs Measurements in the MSSM*, arXiv:1410.4969 [INSPIRE].

[49] R. Barbieri, L.J. Hall and V.S. Rychkov, *Improved naturalness with a heavy Higgs: An Alternative road to LHC physics*, *Phys. Rev.* **D 74** (2006) 015007 [hep-ph/0603188] [INSPIRE].

[50] ATLAS collaboration, *Measurement of the Higgs boson mass from the $H \to \gamma\gamma$ and $H \to ZZ^* \to 4\ell$ channels with the ATLAS detector using 25 fb^{-1} of pp collision data*, *Phys. Rev.* **D 90** (2014) 052004 [arXiv:1406.3827] [INSPIRE].

[51] M. Ciuchini, G. Degrassi, P. Gambino and G.F. Giudice, *Next-to-leading QCD corrections to B —¿ X(s) gamma: Standard model and two Higgs doublet model*, *Nucl. Phys.* **B 527** (1998) 21 [hep-ph/9710335] [INSPIRE].

[52] F. Borzumati and C. Greub, *2HDMs predictions for $\bar{B} \to X_s\gamma$ in NLO QCD*, *Phys. Rev.* **D 58** (1998) 074004 [hep-ph/9802391] [INSPIRE].

[53] F. Borzumati and C. Greub, *Two Higgs doublet model predictions for $\bar{B} \to X_s\gamma$ in NLO QCD: Addendum*, *Phys. Rev.* **D 59** (1999) 057501 [hep-ph/9809438] [INSPIRE].

[54] T. Hermann, M. Misiak and M. Steinhauser, *$\bar{B} \to X_s\gamma$ in the Two Higgs Doublet Model up to Next-to-Next-to-Leading Order in QCD*, *JHEP* **11** (2012) 036 [arXiv:1208.2788] [INSPIRE].

[55] O. Deschamps et al., *The Two Higgs Doublet of Type II facing flavour physics data*, *Phys. Rev.* **D 82** (2010) 073012 [arXiv:0907.5135] [INSPIRE].

[56] D. Eriksson, J. Rathsman and O. Stal, *2HDMC: Two-Higgs-Doublet Model Calculator Physics and Manual*, *Comput. Phys. Commun.* **181** (2010) 189 [arXiv:0902.0851] [INSPIRE].

[57] http://2hdmc.hepforge.org/.

[58] CMS collaboration, *Search for charged Higgs bosons with the H+ to tau nu decay channel in the fully hadronic final state at sqrt s = 8 TeV*, CMS-PAS-HIG-14-020 (2014).

[59] ATLAS collaboration, *Search for charged Higgs bosons decaying via $H^\pm \to \tau^\pm\nu$ in hadronic final states using pp collision data at $\sqrt{s} = 8$ TeV with the ATLAS detector*, ATLAS-CONF-2014-050 (2014).

[60] ATLAS collaboration, *Search for charged Higgs bosons in the τ+jets final state with pp collision data recorded at $\sqrt{s} = 8$ TeV with the ATLAS experiment*, ATLAS-CONF-2013-090 (2013).

[61] CMS Collaboration, *Search for H+ to cs-bar decay*, CMS-PAS-HIG-13-035 (2013).

[62] ATLAS collaboration, *Search for a light charged Higgs boson in the decay channel $H^+ \to c\bar{s}$ in $t\bar{t}$ events using pp collisions at $\sqrt{s} = 7$ TeV with the ATLAS detector*, *Eur. Phys. J.* **C 73** (2013) 2465 [arXiv:1302.3694] [INSPIRE].

[63] LHC HIGGS CROSS SECTION WORKING GROUP collaboration, S. Heinemeyer et al., *Handbook of LHC Higgs Cross Sections: 3. Higgs Properties*, arXiv:1307.1347 [INSPIRE].

[64] B. Coleppa, F. Kling and S. Su, *Charged Higgs Search via $AW^\pm/HW^\pm$ Channel*, arXiv:1408.4119 [INSPIRE].

[65] CMS collaboration, *Search for a heavy charged Higgs boson in proton-proton collisions at sqrts=8 TeV with the CMS detector*, CMS-PAS-HIG-13-026 (2013).

[66] J. Alwall et al., *The automated computation of tree-level and next-to-leading order differential cross sections and their matching to parton shower simulations*, *JHEP* **07** (2014) 079 [arXiv:1405.0301] [INSPIRE].

[67] https://launchpad.net/mg5amcnlo.

[68] R.D. Ball et al., *Parton distributions with LHC data*, *Nucl. Phys.* **B 867** (2013) 244 [arXiv:1207.1303] [INSPIRE].

[69] https://nnpdf.hepforge.org/.

[70] M. Flechl, R. Klees, M. Krämer, M. Spira and M. Ubiali, *Improved cross-section predictions for heavy charged Higgs boson production at the LHC*, arXiv:1409.5615 [INSPIRE].

[71] M. Cacciari, G.P. Salam and G. Soyez, *The Anti-k(t) jet clustering algorithm*, *JHEP* **04** (2008) 063 [arXiv:0802.1189] [INSPIRE].

[72] G. Bevilacqua, M. Czakon, C.G. Papadopoulos, R. Pittau and M. Worek, *Assault on the NLO Wishlist: $pp \to t\bar{t}b\bar{b}$*, *JHEP* **09** (2009) 109 [arXiv:0907.4723] [INSPIRE].

[73] C.G. Lester and D.J. Summers, *Measuring masses of semiinvisibly decaying particles pair produced at hadron colliders*, *Phys. Lett.* **B 463** (1999) 99 [hep-ph/9906349] [INSPIRE].

[74] CMS collaboration, *Measurement of Higgs boson production and properties in the WW decay channel with leptonic final states*, *JHEP* **01** (2014) 096 [arXiv:1312.1129] [INSPIRE].

[75] CMS collaboration, *Search for the Standard Model Higgs boson in the H to WW to lnujj decay channel in pp collisions at the LHC*, CMS-PAS-HIG-13-027 (2013).

[76] CMS collaboration, *Measurement of the properties of a Higgs boson in the four-lepton final state*, *Phys. Rev.* **D 89** (2014) 092007 [arXiv:1312.5353] [INSPIRE].

[77] CMS collaboration, *Search for neutral MSSM Higgs bosons decaying to a pair of tau leptons in pp collisions*, *JHEP* **10** (2014) 160 [arXiv:1408.3316] [INSPIRE].

[78] ATLAS collaboration, *Search for neutral Higgs bosons of the Minimal Supersymmetric Standard Model in pp collisions at $\sqrt{s} = 8$ TeV with the ATLAS detector*, ATLAS-CONF-2014-049 (2014).

[79] CMS collaboration, *Search for an Higgs Like resonance in the diphoton mass spectra above 150 GeV with 8 TeV data*, CMS-PAS-HIG-14-006 (2014).

[80] ATLAS collaboration, *Search for Scalar Diphoton Resonances in the Mass Range $65 - 600$ GeV with the ATLAS Detector in pp Collision Data at $\sqrt{s} = 8$ TeV*, *Phys. Rev. Lett.* **113** (2014) 171801 [arXiv:1407.6583] [INSPIRE].

[81] V. Barger, L.L. Everett, C.B. Jackson, A. Peterson and G. Shaughnessy, *New physics in resonant production of Higgs boson pairs*, arXiv:1408.0003 [INSPIRE].

[82] ATLAS collaboration, *Search For Higgs Boson Pair Production in the $\gamma\gamma b\bar{b}$ Final State using pp Collision Data at $\sqrt{s} = 8$ TeV from the ATLAS Detector*, arXiv:1406.5053 [INSPIRE].

[83] CMS collaboration, *Searches for heavy scalar and pseudoscalar Higgs bosons and for flavor-violating decays of the top quark into a Higgs boson in pp collisions at $\sqrt{s} = 8$ TeV*, arXiv:1410.2751 [INSPIRE].

[84] M. Spira and J.D. Wells, *Higgs bosons strongly coupled to the top quark*, *Nucl. Phys.* **B 523** (1998) 3 [hep-ph/9711410] [INSPIRE].

[85] A. Pomarol and J. Serra, *Top Quark Compositeness: Feasibility and Implications*, *Phys. Rev.* **D 78** (2008) 074026 [arXiv:0806.3247] [INSPIRE].

[86] K. Kumar, T.M.P. Tait and R. Vega-Morales, *Manifestations of Top Compositeness at Colliders*, *JHEP* **05** (2009) 022 [arXiv:0901.3808] [INSPIRE].

[87] S. Jung and J.D. Wells, *Low-scale warped extra dimension and its predilection for multiple top quarks*, *JHEP* **11** (2010) 001 [arXiv:1008.0870] [INSPIRE].

[88] G. Cacciapaglia, R. Chierici, A. Deandrea, L. Panizzi, S. Perries et al., *Four tops on the real projective plane at LHC*, *JHEP* **10** (2011) 042 [arXiv:1107.4616] [INSPIRE].

[89] G.L. Kane, E. Kuflik, R. Lu and L.-T. Wang, *Top Channel for Early SUSY Discovery at the LHC*, *Phys. Rev.* **D 84** (2011) 095004 [arXiv:1101.1963] [INSPIRE].

[90] ATLAS collaboration, *Search for anomalous production of events with same-sign dileptons and b jets in 14.3 fb^{-1} of pp collisions at $\sqrt{s} = 8$ TeV with the ATLAS detector*, ATLAS-CONF-2013-051 (2013).

[91] CMS collaboration, *Search for standard model production of four top quarks in the lepton + jets channel in pp collisions at $\sqrt{s} = 8$ TeV*, arXiv:1409.7339 [INSPIRE].

[92] G. Bevilacqua and M. Worek, *Constraining BSM Physics at the LHC: Four top final states with NLO accuracy in perturbative QCD*, *JHEP* **07** (2012) 111 [arXiv:1206.3064] [INSPIRE].

[93] ATLAS collaboration, *Search for New Physics in events with 4 top quarks in the ATLAS detector at the LHC*, PhD Thesis, Université Blaise Pascal (2013), CERN-THESIS-2013-202.

[94] G. Bevilacqua, M. Czakon, M. Krämer, M. Kubocz and M. Worek, *Quantifying quark mass effects at the LHC: A study of $pp \to b\bar{b}b\bar{b} + X$ at next-to-leading order*, *JHEP* **07** (2013) 095 [arXiv:1304.6860] [INSPIRE].

[95] R.V. Harlander, S. Liebler and H. Mantler, *SusHi: A program for the calculation of Higgs production in gluon fusion and bottom-quark annihilation in the Standard Model and the MSSM*, *Computer Physics Communications* **184** (2013) 1605 [arXiv:1212.3249] [INSPIRE].

[96] http://sushi.hepforge.org/.

[97] M.H. Seymour, *Searches for new particles using cone and cluster jet algorithms: A Comparative study*, *Z. Phys.* **C 62** (1994) 127 [INSPIRE].

[98] J.M. Butterworth, A.R. Davison, M. Rubin and G.P. Salam, *Jet substructure as a new Higgs search channel at the LHC*, *Phys. Rev. Lett.* **100** (2008) 242001 [arXiv:0802.2470] [INSPIRE].

[99] J.F. Gunion, H.E. Haber and J. Wudka, *Sum rules for Higgs bosons*, *Phys. Rev.* **D 43** (1991) 904 [INSPIRE].

[100] M.E. Machacek and M.T. Vaughn, *Two Loop Renormalization Group Equations in a General Quantum Field Theory. 1. Wave Function Renormalization*, *Nucl. Phys.* **B 222** (1983) 83 [INSPIRE].

[101] M.E. Machacek and M.T. Vaughn, *Two Loop Renormalization Group Equations in a General Quantum Field Theory. 2. Yukawa Couplings*, *Nucl. Phys.* **B 236** (1984) 221 [INSPIRE].

[102] M.E. Machacek and M.T. Vaughn, *Two Loop Renormalization Group Equations in a General Quantum Field Theory. 3. Scalar Quartic Couplings*, *Nucl. Phys.* **B 249** (1985) 70 [INSPIRE].

[103] F. Staub, *SARAH 4: A tool for (not only SUSY) model builders*, *Comput. Phys. Commun.* **185** (2014) 1773 [`arXiv:1309.7223`] [INSPIRE].

[104] https://sarah.hepforge.org/.